European Journal of Pharmaceutics and Biopharmaceutics 77 (2011) 469–488

Contents lists available at ScienceDirect

European Journal of Pharmaceutics and Biopharmaceutics

journal homepage: www.elsevier.com/locate/ejpb

Review article

Non-invasive imaging of skin physiology and percutaneous penetration using fluorescence spectral and lifetime imaging with multiphoton and confocal microscopy

Michael S. Roberts [a,b,*], Yuri Dancik [b], Tarl W. Prow [a], Camilla A. Thorling [a,b], Lynlee L. Lin [a], Jeffrey E. Grice [a], Thomas A. Robertson [b], Karsten König [c,d], Wolfgang Becker [e]

[a] The University of Queensland, Therapeutics Research Centre, Brisbane, Australia
[b] The University of South Australia, School of Pharmacy and Medical Sciences, Adelaide, Australia
[c] JenLab GmbH, Saarbrücken, Germany
[d] Department of Biophotonics and Laser Technology, University of the Saarland, Saarbrücken, Germany
[e] Becker & Hickl GmbH, Berlin, Germany

ARTICLE INFO

Article history:
Available online 21 January 2011

Keywords:
Dermatology
Fluorescence lifetime
Penetration
Metabolism

ABSTRACT

New multiphoton and confocal microscope technologies and fluorescence lifetime imaging techniques are now being used to non-invasively image, in space (three dimensions),in time, in spectra, in lifetime and in fluorescence anisotropy (total of 7 dimensions), fluorescent molecules in *in situ* and *in vivo* biological tissue, including skin. The process involves scanning a 2D area and measuring fluorescence at a given tissue depth below the surface after excitation by a laser beam with a wavelength within the one-photon or two-photon absorption band of the fluorophores followed by the stacking together of a series of 2D images from different depths to reconstruct the full spatial structure of the sample. Our aim in this work is to describe the principles, opportunities, limitations and applications of this new technology and its application in defining skin morphology, disease and skin penetration *in vitro* and *in vivo* by drugs, chemicals and nanoparticles. A key emphasis is in the use of fluorescence lifetime imaging to add additional specificity and quantitation to the detection of the various exogenous chemicals and nanoparticles that may be applied to the skin as well as endogenous fluorescent species in the skin. Examples given include equipment configuration; components in skin autofluorescence in various skin strata; imaging and quantification of coexisting drugs and their metabolites; skin pH; nanoparticle zinc oxide skin penetration; liposome delivery of drugs to deeper tissues; and observations in skin ageing and in various skin diseases.

1. Introduction

A goal in studying the skin penetration of compounds in man is to define their disposition kinetics non-invasively *in vivo*. This has proved to be a challenging task, with most work to date relying on destructive sampling using biopsies or excised skin. Pharmacodynamic measures, such as vasoconstrictor assays and laser Doppler assessment of dermal blood flow as well as cutaneous microdialysis, are restricted to events occurring in the dermis. Laser confocal microscopy and multiphoton microscopy (MPM) with multimodal imaging (e.g. reflectance, fluorescence, Raman, photoacoustic, optical coherence tomography) have made possible non-invasive visualisation *in vivo* in the stratum corneum, viable epidermis and dermis. However, we are currently at an early stage in the overall development of these technologies.

In this paper, we examine one of these multimodal imaging technologies, fluorescence lifetime imaging microscopy (FLIM) and its application to the skin. We begin by defining FLIM and its configurations and then show how it can be used to study the skin's morphology, pH and metabolic state and, finally, give examples of skin penetration applications.

2. Fluorescence lifetime

When a molecule absorbs a photon, it enters an excited electronic state. From this state, it can return to the ground state by internally converting the absorbed energy into heat, by passing the energy to another molecule or by emitting a photon. The emission of a photon after excitation is called fluorescence. The general mechanisms involved in absorption and fluorescence emission are shown in Fig. 1.

* Corresponding author. The University of Queensland, Therapeutics Research Centre, School of Medicine, Princess Alexandra Hospital, Woolloongabba, QLD 4102, Australia .Tel.: +61 73 250 2546.

E-mail address: m.roberts@uq.edu.au (M.S. Roberts).

0939-6411/$ - see front matter © 2011 Elsevier B.V. All rights reserved.
doi:10.1016/j.ejpb.2010.12.023

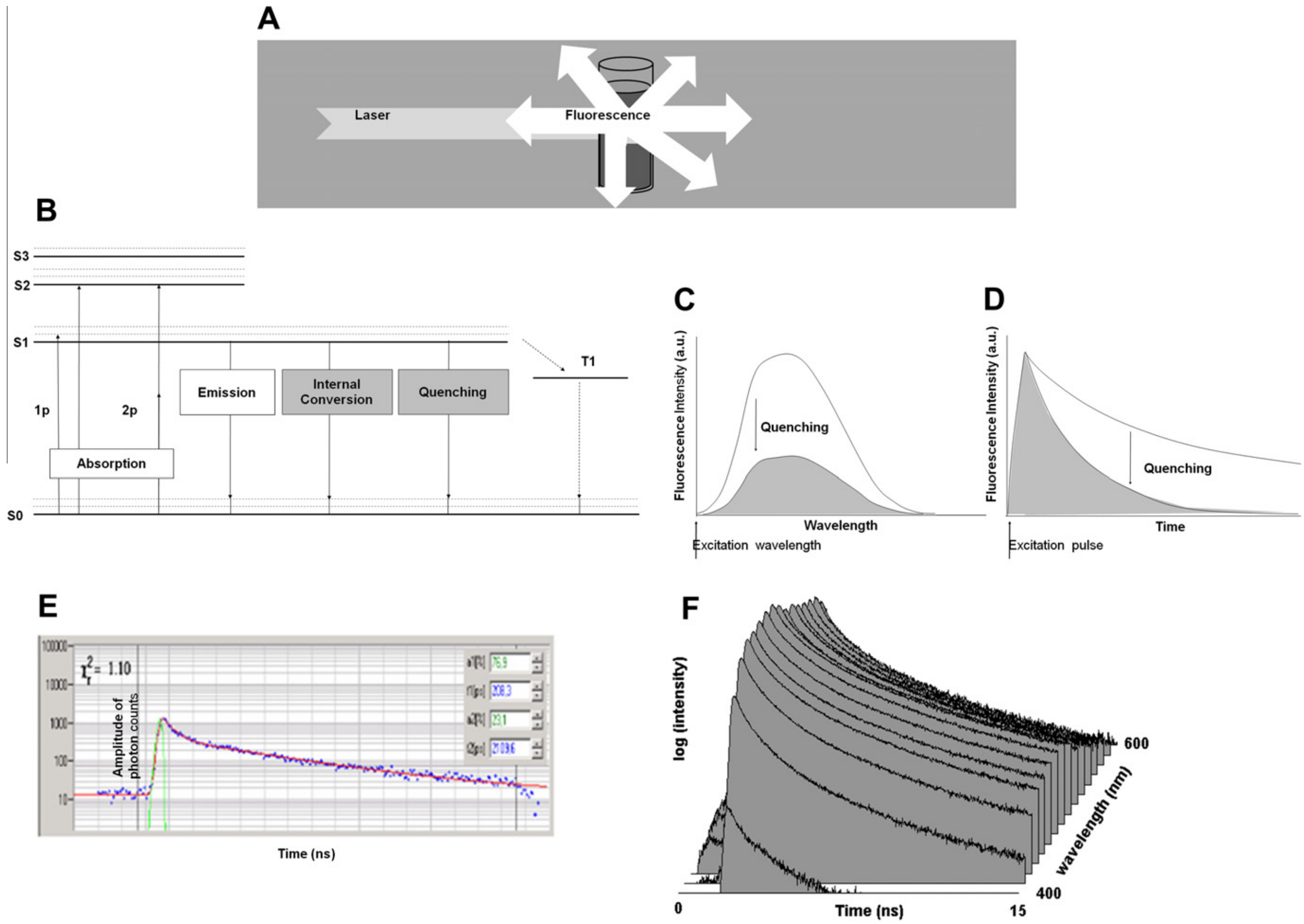

Fig. 1. General principles of fluorescence spectroscopy. (A) On excitation by light, a solute molecule emits fluorescence light in all directions. (B) Jablonski energy diagram. By absorbing light, molecules are excited into a higher electronic state, S1, S2, S3. Higher states, S2, S3, decay into S1 rapidly. From S1, the molecule returns to the ground state, S0, by emitting light, or alternative mechanisms, e.g., internal conversion or quenching. (C) Excitation at appropriate wavelength will yield an emission spectrum characteristic of the type of the molecule. Interaction with the environment can cause fluorescence quenching. Quenching reduces the intensity but does not change the shape of the spectrum. (D) Excitation with short pulses will give a multi-exponential fluorescence decay curve. The fluorescence decay time does not depend on the concentration but decreases with increasing rate of fluorescence quenching. (E) Fluorescence decay curves of biological specimens usually contain several fluorescence components. The result is a multi-exponential decay profile as shown here for two-photon excited fluorescence of human skin. (F) By combining spectral and temporal resolution, the full fluorescence behaviour in the time/wavelength plane is obtained. Adapted from [28]. (For interpretation of the references to colour in this figure legend, the reader is referred to the web version of this article.)

The ground state is S0, the first excited state is S1 (Fig. 1B). By absorbing a photon with energy higher than the gap between S1 and S0, the molecule transits into the S1 state. Higher excited states, S2 and S3, do exist and can be excited, but they decay at an extremely rapid rate into the S1 state. Moreover, the electronic states of the molecules are broadened by vibration and solvent interaction. Therefore, most molecules can be excited by a photon of almost any energy higher than the gap between S0 and S1, but each level reached requires that the specific energy gap is met.

A two-photon process occurs when a molecule is excited by absorbing two photons simultaneously [1]. Here, the total energy that meets the energy gap between S0 and S1 is twice that of the two photons, characterised by an excitation wavelength at about half that for one of original photons. Multiphoton absorption was long seen as only a theoretical possibility. However, it is easily achieved in the focus point of a picosecond or femtosecond laser. Multiphoton excitation has therefore become a standard technique of laser scanning microscopy [2–4]. It should be noted that the probability of absorbing a photon also depends on the angle between the direction of polarisation of the excitation light and the dipole of the molecule. Fluorescence is therefore partially polarised [5]. The degree of polarisation depends on the ratio of the fluorescence lifetime and the rotational depolarisation.

Without interaction with its environment, the molecule can return from the S1 state to S0 by radiation through, for instance, emission of a photon or by internal conversion of the absorbed energy into heat. Moreover, the molecule can interact with its environment and return to the ground state by transferring the energy to another molecule. Effects that let molecules lose their excitation energy to their environment are usually summarized by the term 'fluorescence quenching' (Fig. 1B–D). An excited molecule can also transit into a triplet state, T1. In general, this 'intersystem crossing' or competitive depopulation has little influence on fluorescence lifetime. This process is prominent for the common dyes, such as eosin, methylene blue, certain porphyrins and all PDT compounds used in photodynamic therapy (PDT), is a major pathway for photobleaching and can strongly influence fluorescence lifetime. However, triplet lifetimes can be very long. Excessive triplet population can therefore result in a noticeable depletion of the S1 state and thus in a decrease in fluorescence intensity. High excitation power can result in high triplet population. Moreover, the triplet state is highly chemically reactive. It is therefore important for photochemical reactions, such as photobleaching or singlet-oxygen generation in photodynamic therapy.

If an ensemble of identical molecules is excited, individual molecules end up in different sub-levels of the ground state. Thus, the fluorescence spectrum has a non-zero width. The centre wavelength and the shape of the spectrum are characteristic of the type of the molecule. Because emission, internal conversion and quenching are in competition, the fluorescence intensity changes with the rate constants.

If the same ensemble is excited with short pulses of light, the fluorescence intensity will rise with the excitation pulse and then decay at a characteristic rate. The fluorescence for an isolated molecule is referred to as the radiative lifetime. The fluorescence lifetime is the average time a molecule stays in the excited state and varies for different types of molecules [5,6]. However, the fluorescence lifetime not only depends on the rate constant of the emission path but also depends on the rate constants of the non-radiative decay pathways. These are likely to change when the environment of the molecule changes. The fluorescence lifetime is therefore a direct indicator of the molecular environment of the fluorescent molecules. Unlike the fluorescence intensity, the fluorescence lifetime, within reasonable limits, does not depend on the concentration of the fluorophore. It should be emphasised that the description given above is a simplistic summary. For instance, as evident by the broad absorption and fluorescence emission spectral peaks, absorption not only involves vibrational spectra associated with energy states but also involves solvent-induced inhomogeneous broadening and, in pure solvents, often multiple emission peaks. There are a number of other effects that can influence the fluorescence lifetime. Further, the lifetime also depends on parameters such as local viscosity, solvent polarity, refractive index, aggregation of the fluorophores, proximity to metal surfaces or surfaces of nanoparticles and the presence of electron-transfer partners. Please see [5] and the section following (3) for details.

3. Effects influencing the fluorescence lifetime

The fact that the fluorescence lifetime of a fluorophore depends on its molecular environment but is independent of the fluorophore's concentration provides the unique advantages associated with fluorescence lifetime imaging. The key advantage of fluorescence lifetime techniques is that factors determining the behaviour of molecules in a particular environment, such as in the skin, can be investigated independently of the unknown and usually variable fluorophore concentrations and independently of the presence of absorbers that may change the apparent emission spectra. It should be also noted that intensity-based techniques can be made concentration independent by using 'ratiometric' techniques. These techniques use dyes that emit in two fluorescence emission bands with the intensity ratio being dependent on the local environment. Fluorescence lifetime techniques do not depend on ratiometric dyes (an approach discussed later) and are thus applicable to a wider range of fluorophores, such as the fluorescent proteins and endogenous fluorophores present in biological tissue. Some of the factors that can affect fluorescence lifetime and the application of fluorescence lifetime probing molecular parameters are described below.

3.1. Ions

The fluorescence of fluorophores is quenched by various ions [5]. In fluorescence lifetime imaging, the concentration of the quencher can be directly obtained from the decrease in a solute's fluorescence lifetime because the rate constant for fluorescence quenching is linearly dependent on the concentration of the quencher [5]. A key example in cell biology and especially in defining the function of the neuronal and other systems is Ca^{++} and Cl^{-} [7–10].

3.2. Oxygen

Oxygen is an efficient fluorescence quencher for a large number of fluorophores [5], especially those having a longer fluorescence lifetime. Strong effects are present for pyrene, anthracene and coronene. As these compounds absorb and emit in the UV as well as being relatively water insoluble, they are of limited usefulness in microscopy. Strong quenching is also observed for rare-earth chelates. Unfortunately, the luminescence lifetimes of these compounds are so long – from hundreds of nanoseconds to many microseconds – that they are difficult to use in combination with the fast scanning used in modern laser scanning microscopes.

The most important effect of oxygen is its strong effect on the fluorescence of the endogenous fluorophores NADH and FAD as recognised since the 1930s. Its effect on the redox state can be measured in that the reduced NADH is a natural fluorophore, whilst oxidised NAD^{+} is not. Interestingly, the oxidised form of the other cell redox marker FAD/FADH shows the opposite effect, i.e. FAD is fluorescent, whereas FADH is not. Chance et al. defined a 'redox ratio' that is a direct indicator of the amount of oxygen used in the mitochondria of the cells [11,12]. Effects of oxygen probably exist for other endogenous fluorophores as well [13]. Oxygen-induced lifetime changes can be expected to become important with the introduction of FLIM into clinical applications.

3.3. Binding to proteins, protein configuration

Many fluorescent molecules, including endogenous fluorophores, form complexes with other molecules, particularly proteins. The fluorescence spectra of the different complexes are virtually identical, but the fluorescence lifetimes are usually different. The most likely mechanism is a change in the conformation of the fluorophore, which in turn changes the rate of internal non-radiative decay. When a fluorophore is bound to a protein, the protein configuration may also have an influence on the fluorescence lifetime. For the endogenous fluorophores NADH and FAD, it is known that the lifetimes change on binding to proteins [14,15]. The lifetime changes are substantial, and bound and unbound fractions can easily be distinguished by FLIM (see Table 1). Both the fluorescence lifetimes of the decay components and the relative amplitudes have been found to be sensitive to the metabolic state of cells and tissue [16–19].

3.4. pH sensors

Many fluorescent molecules have a protonated and a deprotonated form. The equilibrium between both depends on the pH. If the protonated and deprotonated forms have different lifetimes, the apparent lifetime is an indicator of the pH. A typical representative of the pH-sensitive dyes is 2′,7′-bis-(2-carboxyethyl)-5-(and-6)-carboxyfluorescein (BCECF) [20]. An example is shown in the application part of this paper.

3.5. Förster Resonance Energy Transfer: FRET

FRET is a dipole–dipole interaction of two molecules in which the emission band of one molecule overlaps the absorption band of the other [21]. In this case, the energy from the first molecule, the donor, can transfer immediately into the second one, the acceptor. FRET can result in quenching of the donor fluorescence and, consequently, in a considerable decrease in the donor lifetime. The energy transfer rate from the donor to the acceptor decreases with the sixth power of the distance. Therefore, it is noticeable only at distances shorter than 10 nm [5]. FRET is therefore used as a tool to investigate protein–protein interaction and to define its intracellular locations with much higher resolution than is possible with a

Table 1
Excitation and emission characteristics of major skin fluorophores (2P denotes two-photon excitation) and collagen second harmonic generation (SHG).

Endogenous fluorophore	Investigated systems	Excitation wavelength (nm)	Emission wavelength (nm)	Fluorescence lifetime (ns)	References
Collagen SHG	*In vivo mouse skin*, tissue model *ex vivo* human skin	730–880 (2P)	1/2 laser wavelength	No lifetime	[73–75]
Elastin	*Ex vivo* rat tissue, *ex vivo* human skin	415 760–830 (2P)	475–575	0.26, 1.96	[74,76]
FAD	*Ex vivo* skin lesions, solution, excised lesions	∼450 ∼800 (2P)	525–550	0.04–0.4 (bound) 2.3–2.8 (free)	[77–79]
Keratin	Keratin solution, skin biopsy, human hair	277 750–800 (2P)	382 450–500	1.4	[80,81]
Melanin	*Ex vivo* skin, *in vivo* melanocytic skin, human hair	730–830 (2P)	∼550	0.1–0.2 0.7–1.4	[31,74,80]
NAD(P)H Free	Cell cultures, *in vivo* hamster pouch check epithelial cells, artificial skin	360 730–800 (2P)	450–460	0.3–0.7	[18,19,82,83]
NAD(P)H Bound	Cell cultures, *in vivo* hamster pouch check epithelial cells, artificial skin	360 730–800 (2P)	450–460	2.5–3.0	[18,19,82,83]
PPIX	*In vivo* chicken embryo membrane, *in vivo* skin lesions	∼ 400 nm	635	5.2 ns, 18–20 ns	[84,85]
Retinol free	Ethanol solution	351 700–830 (2P)	∼ 500	∼1.8, 5.0	[86,87]
Retinol bound	Bound to β-lactoglobulin in ethanol solution	351	N/A	0.7, 3.6, 12	[86]
Vitamin D2, D3	*In vitro* sodium phosphate solution, ethanol solution	290, 350 < 700 (2P)	400–500	N/A	[87,88]

light microscope. Different proteins are labelled with the donor and the acceptor, and FRET is used as an indicator of the binding between these proteins.

The requirements for FRET are, first, an efficient radiationless energy transfer process from an excited, "donor" fluorophore with a sufficiently long lifetime for energy transfer to a non-excited "acceptor" fluorophore [21]. Additional requirements for FRET include that the two fluorophores be within 1–10 nm of each other; that the emission band of one molecule overlaps (>30%) the absorption band of the other; and that the dipole orientations of the donor and acceptor fluorophores be almost parallel. In this case, the energy from the first molecule, the donor, can transfer immediately into the second one, the acceptor. FRET can result in an extremely efficient quenching of the donor fluorescence and, consequently, in a considerable decrease in the donor lifetime.

Other quenching mechanisms can also compete easily at the distances required for FRET. For instance, the fluorescence decay for donor and acceptor fluorophores will also reflect the presence of quenched and nonquenched molecules, with the ratio of these molecules defining the FRET efficiency. Photobleaching can complicate this analysis as, for instance, the acceptor fluorophore would no longer be able to accept energy from the donor fluorophore if it is deliberately photobleached. Indeed, a measurement of the fluorescence intensity of the donor fluorophore before and after bleaching of the acceptor fluorophore has been used to calculate FRET. However, photobleaching carries with it the risk of sample photodamage. The deliberate photobleaching of a specific area in a sample image and the measurement of the recovery time course rate of the photobleached area, as bleached fluorophores diffuse out and unbleached fluorophores diffuse in, are commonly used to estimate the diffusion of the fluorophores in the tissue, a process referred to as Fluorescence Recovery After Photobleaching (FRAP) or as Fluorescence Microphotolysis (FM). Diffusion can also be measured by two other techniques: Fluorescence Correlation Spectroscopy (FCS) that relies on measuring time-dependent Brownian motion-derived intensity fluctuations of fluorophores at low concentrations and scanning Image Correlation Spectroscopy (ICS) where the intensity fluctuations in space can be measured when the scanning rate is much faster than the diffusivity of the fluorophore being measured.

3.6. Second harmonic generation

Second harmonic generation (SHG) is not a fluorescence process but often occurs in combination with multiphoton-excited fluorescence. Unlike fluorescence involving fluorescence radiation from an excited state, SHG occurs when two photons interact with an asymmetric material like collagen in a scattering process to produce a single photon at twice the energy (i.e. at half the excitation wavelength). Hence, SHG is an ultrafast coherent nonlinear process that converts two photons of the incident light into one emitted photon [22]. The wavelength of the emitted photon is exactly one half of the wavelength of the excitation photons. SHG signals show up as ultrafast components in fluorescence decay data recorded in multiphoton microscopes. In biological systems, SHG mainly comes from connective tissue, especially from collagen in animal tissue and from cellulose and starch in plant tissue. The ratio of SHG to autofluorescence intensity in mammalian skin has been used as an indicator of skin ageing [23].

4. Fluorescence decay functions

The fluorescence decay function of an ensemble of similar fluorescent molecules in a homogeneous environment is a single-exponential function. The situation changes if there are several fluorescent species, which may be different molecules, similar molecules of different conformation or similar molecules in different micro-environments. In this case, the resultant fluorescence decay is a sum of several exponentials:

$$F(t) = \sum_{i=1}^{n} I_i e^{-t/\tau_i}, \qquad n > 1 \tag{1}$$

with τ_i being the fluorescence lifetime of the ith species and I_i is the peak intensity, or amplitude, of its contribution. The total peak intensity is the sum of the peak intensities of the individual fluorophores: $I_{peak} = \sum_{i=1}^{n} I_i$. Multi-exponential decay profiles are common in fluorescence lifetime spectroscopy of biological samples (see Fig. 1D). Depending on whether the individual fluorescence components have different spectra, the resulting fluorescence decay profile may or may not vary with wavelength (see Fig. 1E).

In practice, both spectral imaging (defined by emission wavelength) and fluorescence lifetime can be used in quantifying fluorescent molecules. The appropriate combination of techniques in application to a given fluorescent molecule depend on how a given fluorescent molecule responds in a particular environment. For instance, the local pH can be assessed by either using FLIM based on the variations in fluorescent lifetimes of BCECF with pH (as illustrated later in Fig. 7) or using FLIM based on the variation in the emission spectrum for the seminaphtharhodafluors (SNARF dyes). However, whereas FLIM is independent of concentration, intensity-based techniques are not and usually require calibration and the use of more difficult to synthesise 'ratiometric' dyes with two emission bands, the intensity ratio of which depends on the environment. For instance, the carboxy SNARF-1 dye has a p*K*a of ∼7.5

at 37 °C and shows a significant pH-dependent emission shift between yellow-orange (acid) to deep-red fluorescence (basic). Accordingly, the ratio of its fluorescence intensities at two emission wavelengths (often 580 nm and 640 nm) can be used to define the local pH.

There is yet a third method that is most applicable for fluorescent proteins, fluorescence anisotropy. A very large molecule will be expected to emit fluorescence parallel to the linearly polarised laser excitation source for a confocal microscope and therefore has a high fluorescence anisotropy (i.e. directionally dependent fluorescence). On the other hand, if this protein fluorophore was cleaved by an enzyme into small fragments that tumble (Brownian motion) readily, fluorescence perpendicular to the excitation polarised light will increase significantly. The decrease in the relative intensities of polarised parallel and perpendicular light emission defines lower fluorescence anisotropy. Low anisotropy regions in a spatiotemporal map for a given fluorescence emission indicate regions of high enzyme activity.

Thus, the methodology to be defined is dependent on what question is being asked and what probes can be used for a given specimen without creating artefacts. For instance, is the probe non-toxic, a membrane permeant, is there a concentration-dependent effect, does it affect autofluorescence or modify its measurement specificity, is there depopulation radiation kinetics (S2, S3–S0; Fig. 1B) that may lead to, for example, non-exponential decays? Further, there may be changes either in the probe fluorescence properties (e.g. quenching, emission wavelength and lifetime) or those of the biological system, such as pH, viscosity, and in autofluorescence as a result of a probe–biological system interaction. Hence, it should be emphasised that many interactions can modify fluorescent behaviour and the best technique should be employed. FLIM is but one of these.

5. Fluorescence lifetime imaging microscopy

Fluorescence lifetime imaging microscopy in Life Sciences was introduced more than 20 years ago [24]. The instrument used for the work presented here is based on a DermaInspect system for clinical multiphoton fluorescence tomography of skin (Jenlab, Germany) [25] and an SPC-830 TCSPC FLIM module from Becker & Hickl, Germany [26]. The basic technical principles used in these instruments are described below.

5.1. FLIM technique

There are several FLIM techniques. These can be classified into time domain, frequency domain, photon counting, analog, point-scanning and wide-field imaging techniques. The methods differ in their photon efficiency, i.e. in the number of photons required for a given lifetime accuracy, their ability to resolve the parameters of multi-exponential decay functions, capability to record signals in several wavelength channels and compatibility with fast scanning modalities. Commonly used FLIM techniques, their essential parameters and typical applications are reviewed in [27].

For the applications presented here, we used FLIM by multi-dimensional time-correlated single-photon counting (TCSPC) in combination with multiphoton laser scanning because it provides single-photon sensitivity, excellent time resolution with the capability to resolve multi-exponential decay profiles and depth resolution. Moreover, TCSPC FLIM is compatible with fast scanning and capable of recording FLIM data in several wavelength channels simultaneously.

The principle of TCSPC FLIM is shown in Fig. 2. The technique is based on excitation with a high-frequency pulsed laser, detection of single photons of the fluorescence light, measurement of the lifetimes of the emitted photons resulting from the excitation light pulses, determination of the location of the laser spot in the sample at the moment of photon detection and build-up of a multi-dimensional photon distribution over these parameters [26,28]. The result of imaging over a two-dimensional (2D) area is an array of pixels defined by the distribution of Lifetime data over the 2D space. Embedded in each pixel are lifetime data that define numbers of photons collected at various times after the pulsed light excitation. This means that each pixel contains a full fluorescence decay curve. As shown in Fig. 2B, the technique can be extended to simultaneous detection in several wavelength channels. In that case, the wavelength of the photon is added as an additional parameter of the photon distribution build-up. The resulting data consists of an array of pixels, each of which contains a number of decay curves for different wavelengths (see Fig. 2C, middle and right). The instrument used for the work presented here (Fig. 2A) has four wavelength channels with individual photomultiplier (PMT) detectors [29]. Up to 16 wavelength channels can be obtained by using a multi-anode PMT [26,28,30,31].

5.2. Optical system

To obtain a functional TCSPC FLIM system, the principle shown in Fig. 2 has to be combined with a scanning system. Moreover, there has to be a pulsed excitation source with a high repetition rate. The laser may excite the fluorescence in the sample via one-photon excitation or multiphoton excitation. For FLIM detection, there is no difference between the excitation principles. There are, however, significant differences in the optical systems.

Single-photon excitation uses an ultraviolet or visible light laser. The laser beam excites fluorescence within a double cone throughout the whole depth of the sample. Detecting all the fluorescence returned from the sample would result in a conventional image, i.e. the image of the focal plane would be overlaid by blurry images of sample layers above and below the focal plane. The fluorescence light is therefore focused into a confocal pinhole in the upper focal plane of the microscope. Only light from the focal plane is focused into the pinhole and thus able to pass it [4]. Typical excitation power for biological samples is on the order of a few 10 μW in the sample plane, and therefore, one-photon FLIM systems normally use picosecond diode lasers. One-photon FLIM is available for most of the existing laser scanning microscopes. For conventional microscopes, confocal scanners with TCSPC FLIM detection systems are available [26,32]. One-photon FLIM has been combined with scanners for clinical tissue imaging, such as in the Vivascope of Lucid Inc., Rochester, and with ophthalmic scanners [13,26,33].

Multiphoton excitation uses a femtosecond Titanium:Sapphire (Ti:Sa) laser to excite the sample by multiphoton absorption. Simultaneous absorption of two (or more) photons was theoretically predicted by Göppert-Mayer [1]. It was suggested for laser scanning microscopy by Wilson and Sheppard in 1984 [34] and introduced in practice by Denk and Strickler [2] in 1990. Two-photon excitation has a number of advantages over one-photon excitation.

First, absorption by the sample at the NIR wavelength of the Ti:Sa laser is low. Also the scattering coefficient is lower than at visible or ultraviolet wavelengths. Two-photon excitation can therefore be used to excite fluorescence in deep tissue layers [2–4,35].

Second, noticeable absorption and fluorescence excitation occur only in the focus of the microscope lens. Thus, two-photon excitation intrinsically obtains depth resolution and suppression of out-of-focus fluorescence. In contrast to one-photon excitation with

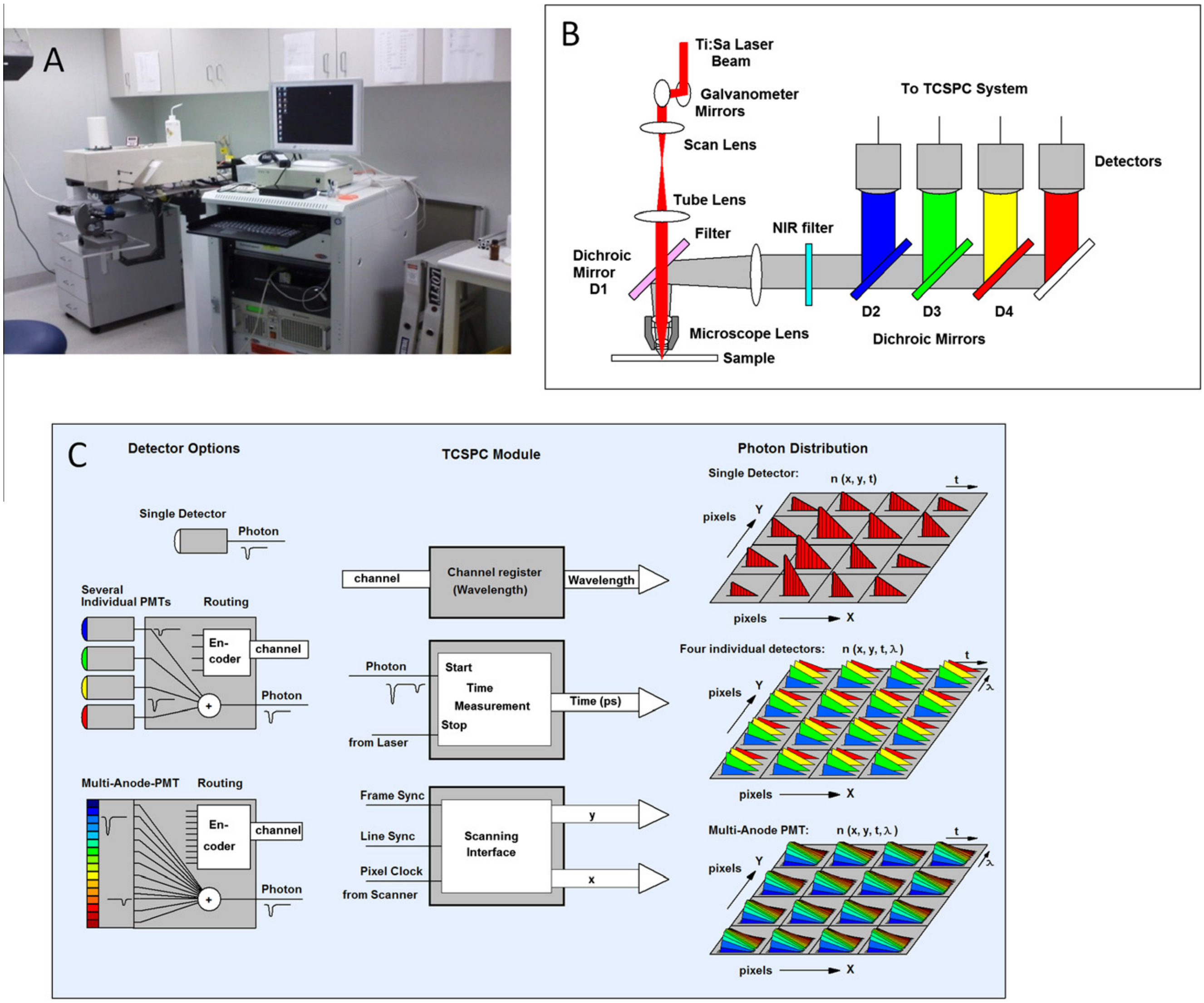

Fig. 2. (A) DermaInspect with TCSPC FLIM. (B) Optical principle of multiphoton non-descanned detection scanning system (C) Principles behind TCSPC FLIM showing the options of a single photomultiplier (PMT), 4 PMTs corresponding to 4 emission bands and an array of PMTs for 64 emission bands; the module; and the space, time, and spectral bands. It is observed that a single PMT has a single band (represented by red/black colour), 4 PMTs 4 bands (represented by red/black, yellow, green and blue colours) and the array 64 bands/colours.

confocal detection, which avoids out-of-focus *detection*, two-photon excitation avoids out-of-focus *excitation*.

The fact that the fluorescence signal comes only from the focal point leads to a third advantage of multiphoton excitation. Because no pinhole is needed to reject out-of-focus light, a multiphoton microscope is able to detect photons that are scattered on the way out of the sample. The ability to detect such photons leads to a substantial increase in detection efficiency for deep sample layers. The basic optical principle of our multiphoton fluorescence microscopy system is shown in Fig. 2B. The angle of the Ti:Sa laser beam is scanned by two fast-moving galvanometer mirrors. The scan lens projects the axis of the galvanometer mirrors on the microscope lens. Thus, the angle of the beam at the microscope lens changes with the scanning. The laser focus therefore scans an image area in the sample. The fluorescence light from the sample is collected back through the microscope lens and separated from the laser beam by a dichroic mirror, D1. The beam of fluorescence light is further split into four spectral components by dichroic mirrors, D2–D4. The spectral components are detected by PMTs, and the signals are sent to the TCSPC electronics.

5.3. FLIM data analysis

To analyse the FLIM data, we used the SPCImage FLIM data analysis software from Becker & Hickl, Germany [32]. The principles of the procedures used by SPCImage are as follows. TCSPC FLIM data can be considered as an array of pixels, each containing a large number of time channels spread over the fluorescence decay. In other words, the FLIM measurement delivers images with a decay curve in each pixel (see Fig. 3A). Several such arrays may exist if several detectors or detector channels are used.

To obtain fluorescence lifetimes, the decay curves in the individual pixels are fitted with an appropriate decay model function (Eq. (1)). In recognising that the time resolution of the measurement system is finite, the fitting routine also accounts for the 'instrument response function' (IRF). The IRF is the pulse-shape and the FLIM system would record for an infinitely short fluorescence lifetime. The fitting procedure convolutes the model decay function with the IRF and normalises the parameters so that the predicted area under the curve is the same as the measured fluorescence decay profile. This is an iterative process in which the normalisation of the area is repeated as the model parameters

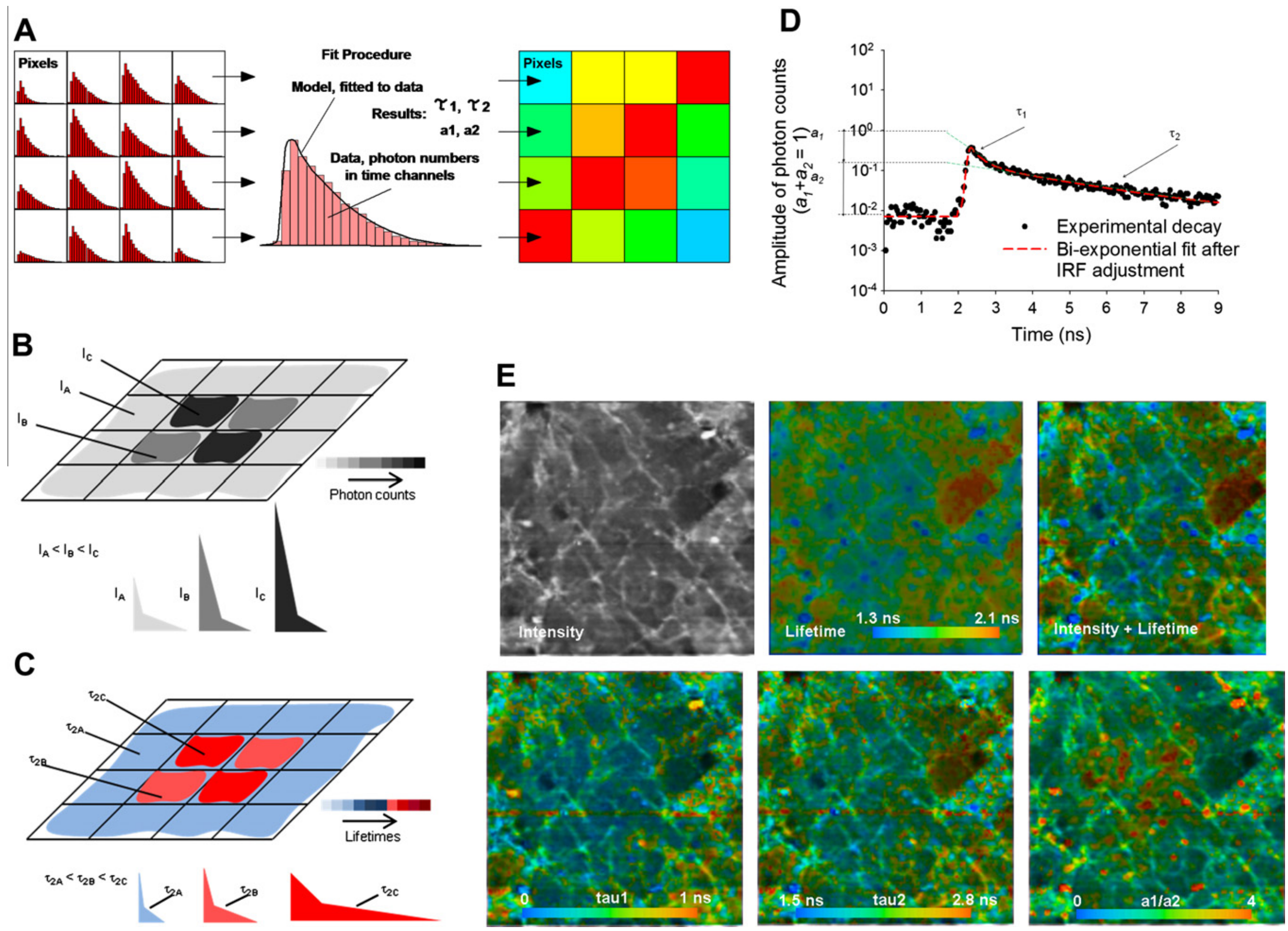

Fig. 3. Analysis of FLIM data. (A) Left: Raw data, pixels contain decay curves. Middle: Fit procedure, delivers lifetimes and amplitudes of decay components for individual pixels. Right: Lifetime data: Pixels contain results of fit procedure. (B) Expressing intensity as an (x, y) gray scale plot where the brightness is based on the peak intensity defined by the peak total number of photons emitted per pixel after a pulse of light. (C) Expressing the long lifetimes (τ_2) for pixels in an (x, y) plot. (D) Process of obtaining lifetime parameters for short (τ_1) and long (τ_2) and corresponding amplitudes (a_1 and a_2) from FLIM data by a nonlinear, bi-exponential regression of an experimental decay curve, after adjusting for instrument response function, IRF. (E) Actual intensity and lifetime images of human stratum corneum. Upper row: Combination of the intensity and the lifetime information. Left: Intensity image, brightness represents total number of photons per pixel. Middle: Pure lifetime image, colour represents fluorescence lifetime. Right: Combined image, brightness represents number of photons, colour represents fluorescence lifetime. Lower row: Double-exponential decay analysis. Left to right: Images showing the decay time of the fast lifetime component, the decay time of the slow lifetime component, and the ratio of the intensity coefficients of the lifetime component.

are varied so that the convoluted model function best fits the measured decay curve. The entire regression procedure is performed in all pixels of the image.

Typical models of fluorescence decay data are single exponentials or a sum of exponential terms (Eq. (1)). The models are normally characterised by several parameters, e.g. the fluorescence lifetimes in the exponential terms and their amplitudes. The fitting procedure delivers these parameters for all pixels of the scan (Fig. 3A, left). The pixels of the resulting lifetime data array contain the results of the fitting procedure (Fig. 3A, middle, right).

In the simplest case, the decay curves of the individual pixels can be characterised by a single-exponential model. The result of the fitting procedure is then a single fluorescence lifetime. Lifetime images created from such data use the number of photons per pixel (the intensity) as brightness (Fig. 3B) and the fluorescence lifetime as colour (Fig. 3C). An example of combining both into the final image is shown in Fig. 3E, upper row.

However, fluorescence decay curves of biological samples usually contain fluorescence components of several fluorescing species. The decay curves are then multi-exponential.

Fig. 3D shows an example of an experimental decay curve that is fitted by a double-exponential model,

$$N(t) = a_1 e^{-t/\tau_1} + a_2 e^{-t/\tau_2} \tag{2}$$

where $N(0) = a_1 + a_2 = 1$. Fitting the decay curves with this model delivers the lifetimes, τ_1 and τ_2, and the amplitudes, a_1 and a_2, as shown in Fig. 3D.

The analysis software provides a number of options for the display of individual parameters. It can assign either τ_1, τ_2, a_1 or a_2 to the colour of the display or use ratios such as τ_1/τ_2 or, a_1/a_2. An example of using these parameters to characterise autofluorescence of human stratum corneum is shown in the lower row of Fig. 3E. As discussed in more detail later, the major autofluorescent component in the skin, nicotinamide adenine nucleotide, NADH (often expressed as NAD(P)H to recognise the possible presence of NADPH that has identical fluorescence but exists at low levels), exists mainly in the cytoplasm in the free unbound form and in the mitochondria as a bound form to mitochondrial enzymes (Table 1). Exposure of the skin to foreign oxidants may lead to the oxidation of the fluorescent NADH to the non-fluorescent NAD^+ with an increase in free NAD(P)H (increase in a_1), a decrease in bound NAD(P)H (decrease in a_2) and an increase in the free to bound NAD(P)H ratio (increase in ratio a_1/a_2). In addition, if the foreign insult has also led to a change in the pH, oxidation state etc. in the cells, there may also be a change in the free, fast NAD(P)H lifetime (τ_1), in the bound, slow NAD(P)H lifetime (τ_2) or in the ratio of lifetimes (τ_1/τ_2). In general, ratios of either intensity (a_1/a_2) or lifetimes are more sensitive at reflecting redox changes in cells than individual amplitude (a_1, a_2) or lifetime (τ_1, τ_2) values. Further, unbound NADH can exist in folded and extended conformations. The extent of bound NADH and its lifetime reflects NADH's cycling through the mitochondria's cell energy production pathways, with the varying sizes of the enzymes being bound, contributing to the observed fluorescence anisotropy [36]. As a consequence, changes in the fluorescence anisotropy of NAD(P)H can also reflect the effects of external stresses on the skin.

Moreover, the software can calculate the commonly used amplitude-weighted (mean) lifetime

$$\tau_m = a_1\tau_1 + a_2\tau_2 \qquad \text{where} \quad a_1 + a_2 = 1$$

or the intensity-weighted lifetime

$$\tau_i = \frac{a_1\tau_1^2 + a_2\tau_2^2}{a_1\tau_1 + a_2\tau_2}$$

of the double-exponential decay and assign these parameters to the colour of the image. It should be noted that τ_m is identical to the normalised zeroth moment of $N(t)$ ($\tau_m = \int N(t)\,dt$), whereas τ_i is identical to the normalised first moment of $N(t)$, i.e. $\tau_i = \frac{\int t\,N(t)\,dt}{\int N(t)\,dt}$.

Reporting of data as either amplitude-weighted (mean) or intensity-weighted lifetime depends on the application. It is to be noted that fluorescent molecules with long lifetimes have a greater quantum yield (i.e. are brighter) and will contribute more to values for intensity-weighted than the amplitude-weighted lifetime, where the short lifetime components are more strongly weighted. Hence, an intensity-weighted lifetime is the closest approximation to an assumed single-exponential approximated lifetime. As an example of these effects, the appearance of a short lifetime component at 0.6 ns in the formation of a binary mixture from two phases with similar lifetimes of ~2.6 ns results in a shorter amplitude-weighted lifetime (~2.2 ns) but approximately the same intensity-weighted lifetime (~2.6 ns) [37]. Hence, amplitude-weighted lifetimes are often used in: a) FRET experiments to represent the classic FRET efficiency obtained by steady-state FRET techniques and b) being more sensitive to fast decay components, to display changes in the composition of the decay, e.g. bound–unbound ratios of NADH and FAD. Accordingly, an advantage of FLIM is an ability to use the amplitude-weighted lifetime to measure the concentration of fluorescent molecules, independent of the individual component quantum yields. An overview of the data analysis principles used and the corresponding software is given in [28].

6. FLIM as an indicator of the molecular environment and metabolism

6.1. Endogenous fluorophores

An example of FLIM of endogenous fluorophores is shown in Fig. 4. The images were recorded simultaneously in several wavelength channels, as described in Section 3. The images were taken from human epidermis and recorded in wavelength intervals from 350 to 450 nm, 450 to 515 nm and 515 to 620 nm. The excitation wavelength was 740 nm. Fluorescence decay data in a selected pixel are shown in the lower row.

Fluorescence in biological tissues originates from a number of autofluorescent molecules, allowing *in situ* imaging of, for example, keratin, elastin in the stratum corneum, FAD, protoporphorin IX (PpIX), free and protein-bound NAD(P)H in viable epidermis and collagen in dermis (Table 1). It is evident that for many of these molecules, selectivity is also given by an appropriate choice of emission wavelength band. Fig. 4 shows an example of multichannel FLIM imaging in skin at the stratum granulosum level. Three example images and decay curves from a selected pixel are shown in the upper and lower panels, respectively. The decay curves have been fitted with a bi-exponential model, shown as a solid line. The common fluorophores present in the stratum granulosum are NAD(P)H and FAD. The left panel, 350–450 nm, shows primarily NAD(P)H, and the centre panel contains both NAD(P)H and FAD signals. These images were taken with 740-nm excitation light, which works well for NAD(P)H on our system. However, this is

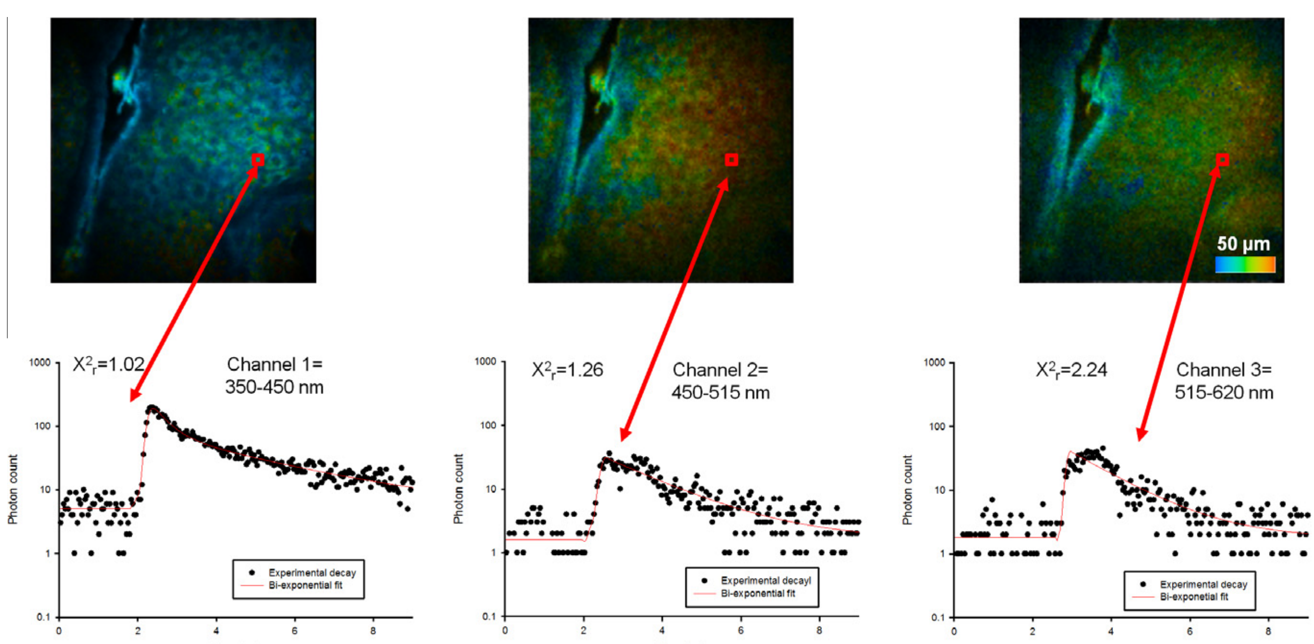

Fig. 4. FLIM data recorded simultaneously in three of the four wavelength channels. Upper row, left to right: Lifetime images in wavelength intervals 350–450 nm, 450–515 nm, 515–620 nm. Lower row: Fluorescence decay data in selected pixel.

not the optimal excitation wavelength for FAD, as indicated by the lack of cellular definition in the right panel (Channel 3, 515–620 nm). In this case, the FAD signal is weak but present. The decay curves also show that fewer and fewer photons are being collected at the higher emission wavelengths (solid dots). Fig. 4 highlights the capacity for FLIM to be used to detect multiple fluorophores simultaneously and the use of decay curves in combination with images to determine optimal settings for complex analysis.

An application of double-exponential decay analysis to multiphoton FLIM data of human skin is shown in Fig. 5. Images showing the lifetimes of the decay components (τ_1, τ_2), ratios of the lifetimes (τ_1/τ_2) and ratios of the amplitudes (a_1/a_2) of the double-exponential decay in a plane with the stratum corneum and the viable epidermis of a volunteer are shown in Fig. 5A and B, respectively.

The challenge then is interpreting the resulting (x, y) profiles. It is evident, for instance, that the lifetimes in the intercellular spaces in both the stratum corneum and viable epidermis differ from those inside the cells. The mean values in the short τ_1 and long τ_2 lifetime epithelial (x, y) profiles (Fig. 5B) are consistent with reported lifetimes for free and protein-bound NADH in normal hamster cheek pouch epithelial cytoplasm of 290 ps and 2.03 ns, respectively [19]. Ghukasyan et al. [18] and Skala et al. [19] have shown the lifetime of NADH changes upon binding in epithelial cells *in vivo* and in cultures, respectively. These studies suggest that changes in the amount of free and protein-bound NAD(P)H can reflect changes in overall metabolism. In practice, this translates to the a_1/a_2 ratio being an indicator of metabolism that is inversely related. A decrease in the protein-bound NAD(P)H contribution (a_2) would yield a larger a_1/a_2 value and has been associated with serum starvation and cyanide treatment, both resulting in decreased metabolic rate [16]. Therefore, NAD(P)H contribution ratios can be utilized to suggest metabolic rate changes when compared with correct control groups.

6.2. Exogenous fluorophores and their metabolites

A key difficulty in analysing any exogenous fluorophore is the presence of autofluorescence. Fig. 5C shows that the phosphorescence emission of zinc oxide (ZnO) nanoparticles can be separated from the autofluorescence in skin using an appropriate spectral band. The spectra and lifetimes of exogenous fluorophores are also markedly affected by their environment [5,38]. Fig. 6 illustrates this effect with the diagnostic agents fluorescein and rhodamine. The lifetime of fluorescein in PBS varies markedly with the pH of the solution (Fig. 6A). The lifetimes of the rhodamine B zwitterions and rhodamine cation are strongly dependent on the solvent (Fig. 6B).

Since fluorescence lifetime is a signature property for a given fluorophore, FLIM can be very useful in differentiating a parent compound from its metabolite(s). Fluorescein and its metabolite fluorescein glucuronide have similar peak excitation wavelengths (Fig. 6C) and cannot be distinguished on the basis of this parameter (Fig. 6D and [39]). Their fluorescence lifetimes, however, differ significantly, as shown in Fig. 6E. Using fluorescein and fluorescein

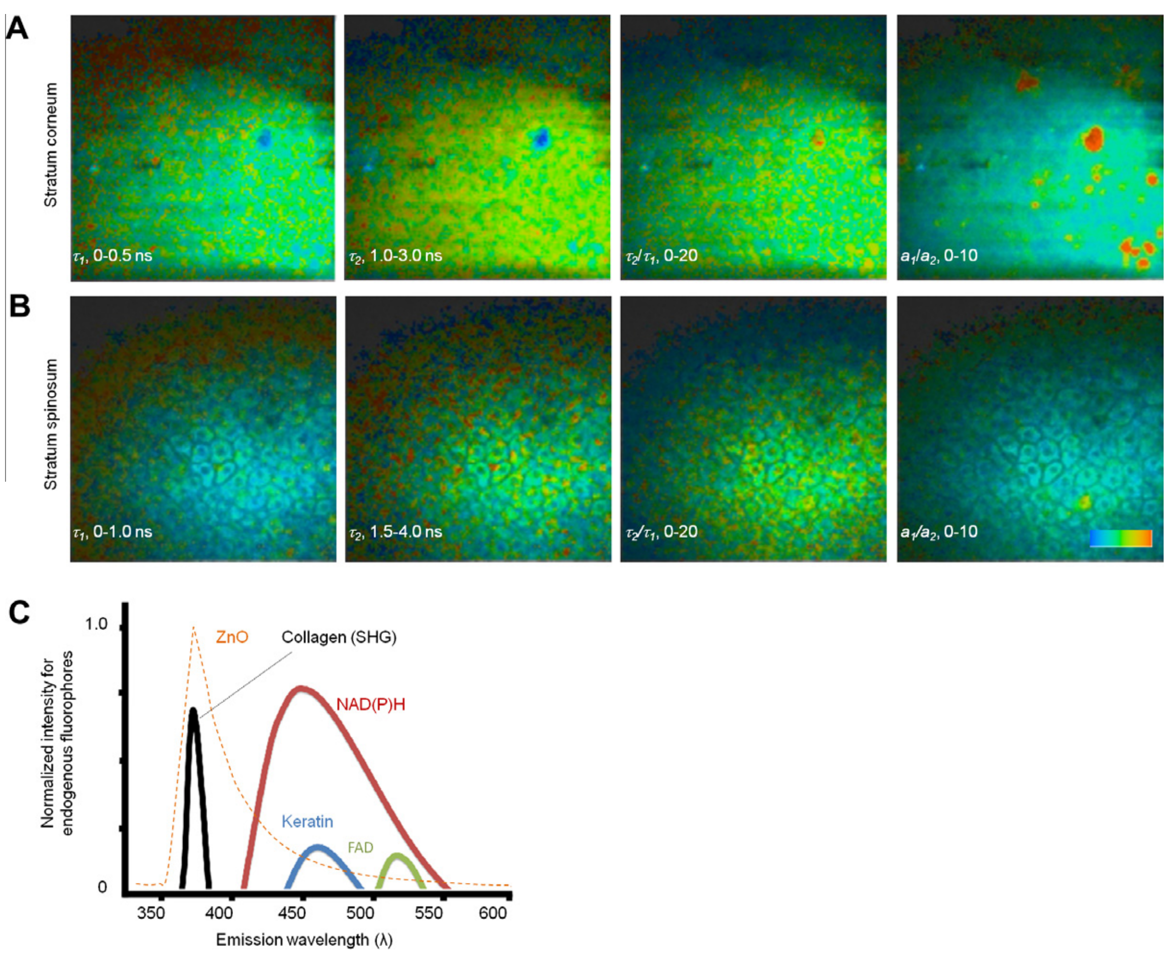

Fig. 5. Multiphoton lifetime images taken at different layers of human skin, double-exponential decay analysis, (A) Stratum corneum. (B) Stratum spinosum. Left to right: Lifetime of fast decay component, lifetime of slow decay component, ratio of both, ratio of amplitudes of the decay components. (C) Normalised emission spectra of endogenous cutaneous fluorophores and zinc oxide (ZnO).

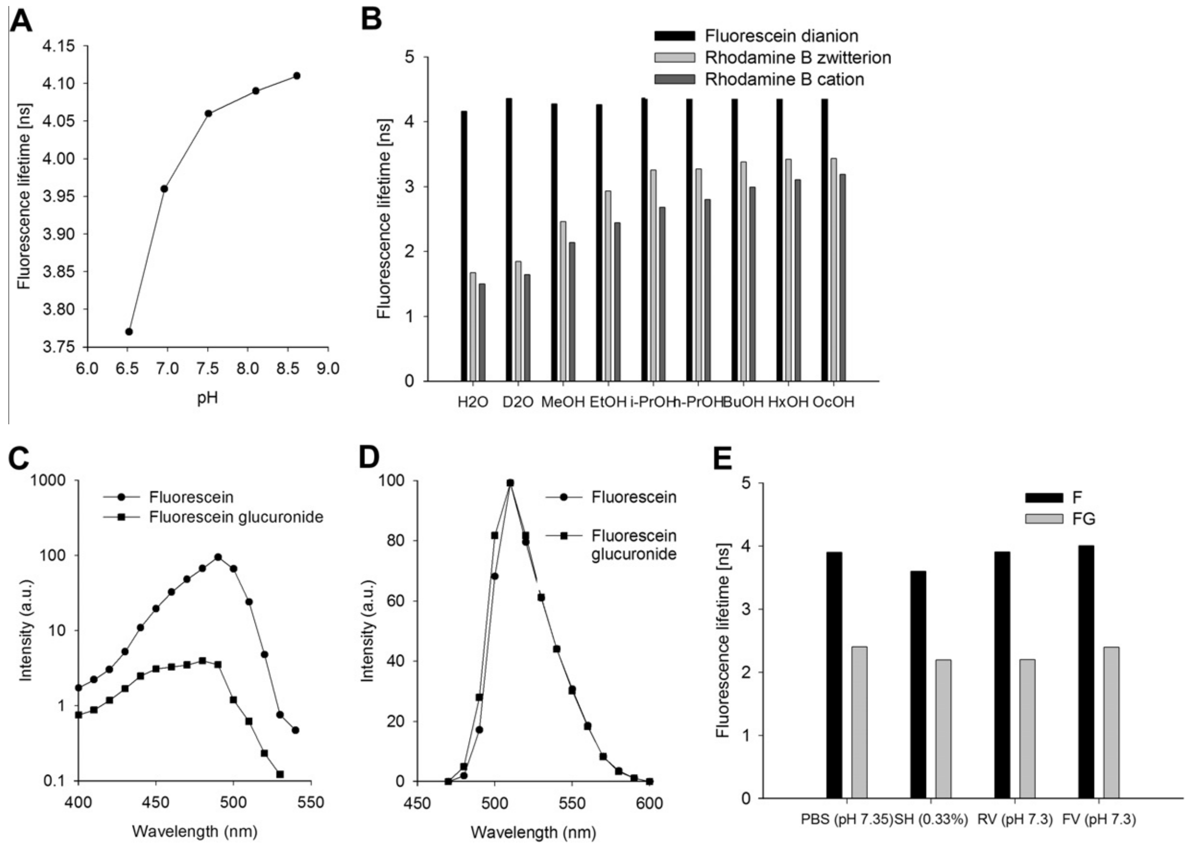

Fig. 6. Fluorescence lifetime changes according to the environment the fluorophores. (A) The lifetime of fluorescein in PBS (1:150,000) depends on the pH of the solution; data adapted from [89]. (B) The lifetimes of the rhodamine B zwitterion and cation, unlike that of the fluorescein dianion, are strongly dependent on the solvent (H_2O = water, D_2O = deuterated water, MeOH = Methanol, EtOH = Ethanol, i-, n-PrOH = i-, n-Propanol, BuOH = n-Butanol, H*x*OH = n-Hexanol, OcOH = n-Octanol). Data adapted from [90]. (C) Excitation spectra for fluorescein and fluorescein glucuronide at pH 7.3 for an emission wavelength of 515 nm. [90]. (D) Emission spectra for fluorescein and fluorescein glucuronide at pH 7.3 for an excitation wavelength of 495 nm [85]. (E) FLIM allows parent drugs and metabolites to be identified. The lifetime of the diagnostic agent fluorescein is 3.6–4.0 ns, whereas that of its metabolite fluorescein glucuronide is 2.2–2.4 ns in phosphate-buffered solution (PBS), sodium hyaluronate (SH) and human raw vitreous (RV) and filtered vitreous (FV). Data adapted from [91]. (F) Human epidermis *in vivo* after application of fluorescein to stratum corneum–stripped skin.

glucuronide as example of fluorophores, Roberts et al. have shown that it is possible to exploit the differences in lifetimes of parent drugs and their metabolites to study drug elimination and metabolism kinetics in tissues *in vivo* [40].

We have also applied fluorescein to human epidermis *in vivo* after stripping of the stratum corneum and observed its fluorescence over time. Fig. 6F shows a typical example. It is evident that with 920 nm excitation there is no background fluorescence allowing fluorescein alone to be observed. Fig. 6F shows that fluorescein is mainly transported between the epidermal cells after topical application and does not reach the dermis until about 30 min after application, at which time the dermal papillae become clearly observable.

6.3. pH imaging

One application of FLIM is to use the different fluorescence lifetimes of an exogenous compound in the protonated and deprotonated forms to define the pH in the various regions of the stratum corneum. For instance, the compound 20,70-bis-(2-carboxyethyl)-5/6-carboxyfluorescein (BCECF) has a shorter lifetime in the deprotonated state at lower pH values (Fig. 7). Hanson et al. [41] used BCECF to show that skin pH was lower at the skin surface microdomains of the extracellular matrix than in intracellular spaces of corneocytes in hairless mouse stratum corneum. A similar profile occurs for artificial human skin constructs as shown in Fig. 7.

7. Investigating protein interaction by FRET

Because of its dependence on distances on the molecular scale, FRET has become an important tool of cell biology [42]. Different proteins are labelled with the donor and the acceptor; FRET is then used to verify whether the proteins are physically linked and to determine distances on the nanometre (nm) scale.

The use of FLIM for FRET experiments has the obvious benefit that the FRET intensity can be obtained from a single lifetime image of the donor. Donor bleedthrough and directly excited acceptor fluorescence [42] therefore have no influence on FLIM–FRET measurements. The only reference value needed is the donor lifetime in absence of the acceptor [28,29,43,44].

It has been shown that for a given efficiency of the optical system and detector and a given excitation power, FLIM-based FRET measurements give better accuracy than steady-state techniques [45]. FLIM with single-exponential decay analysis does not, however, solve the 'stoichiometry problem'. The conventional 'FRET efficiency' depends both on the distance between donor and acceptor and on the fraction of interacting donor molecules. In the simplest case, a fraction of the donor molecules may not be linked to their targets, or not all of the acceptor targets may be labelled with an acceptor. This can happen especially in specimens with conventional antibody labelling. But even if the labelling is complete, not all of the labelled proteins in a cell may interact and the fraction of interacting protein pairs varies throughout the cell.

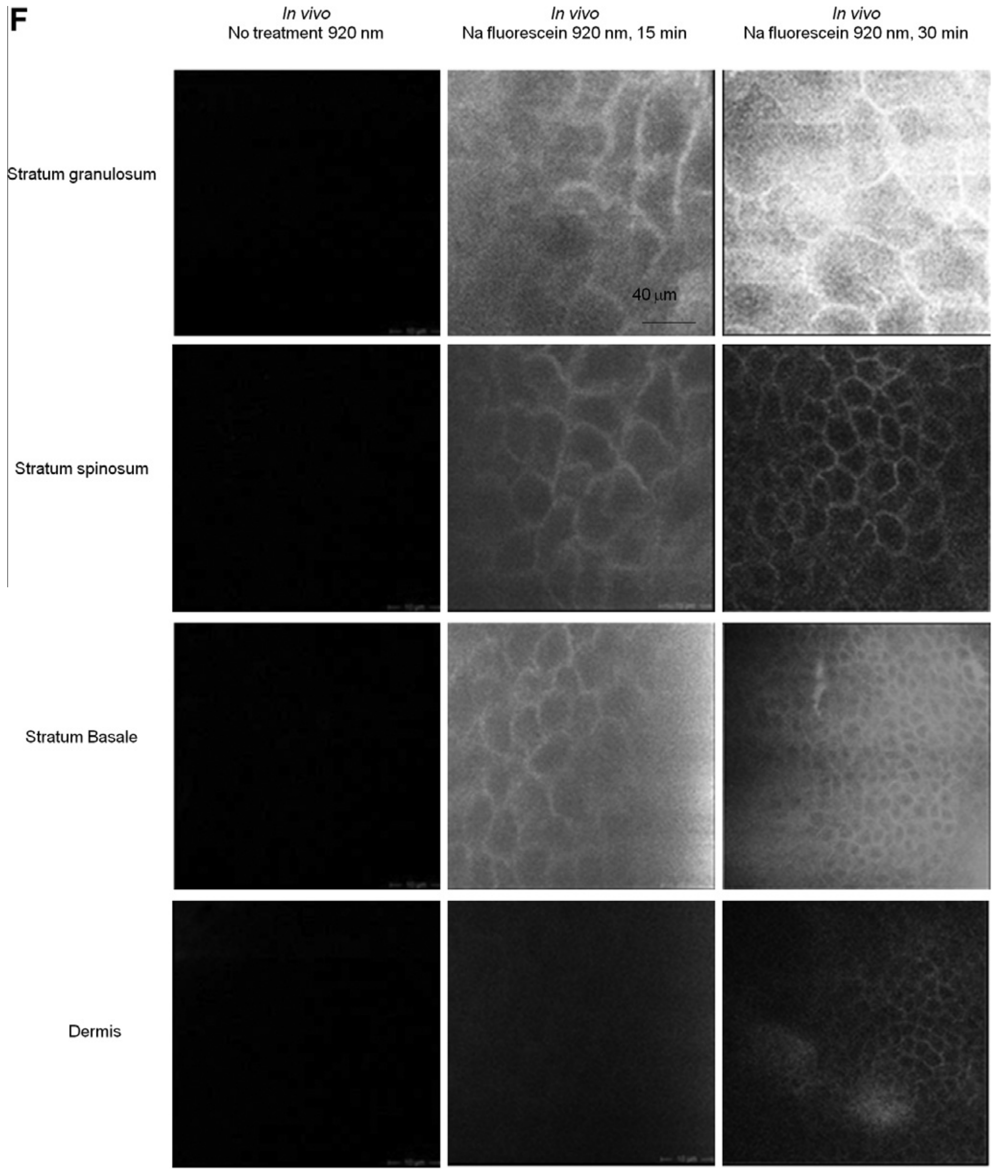

Fig. 6 (*continued*)

TCSPC FLIM solves the problem of interacting and non-interacting donor by double-exponential lifetime analysis [28,29,46,47]. The resulting donor decay functions can be approximated by a double-exponential model, with a slow lifetime component from the non-interacting (unquenched) and a fast component from the interacting (quenched) donor molecules. If the labelling is complete, as can be expected if the cell is expressing fusion proteins of the GFP variants, the decay components directly represent the fractions of interacting and non-interacting proteins (a small correction for the notoriously unknown orientation factor κ^2 [5] may be still required). The composition of the donor decay function is illustrated in Fig. 8A. The a_1/a_2 ratio directly delivers the ratio of interacting and non-interacting donor molecules. The distance between donor and acceptor is obtained from the ratio of the lifetimes of the interacting and non-interacting donor fractions, τ_{fret}/τ_0, via the Förster formula. Interestingly, the technique does not require any external reference standard. The reference is the lifetime of the non-interacting donor, τ_0. Because this comes from the same data set as τ_{fret}, the technique is less sensitive to variations in the local environment of the donor than other FRET techniques.

Fig. 8B shows the result of a double-exponential analysis of FLIM–FRET data. The images show a cultured human embryonic kidney (HEK) cell expressing two interacting proteins labelled with CFP and YFP. The left image shows the ratio of the lifetimes of the non-interacting and interacting donor fractions, τ_0/τ_{fret}. The distribution of τ_0/τ_{fret} in different regions is shown far left. The locations of the maxima differ by only 10%, corresponding to a distance variation of only 2%. However, the variation in the intensity coefficients, a_1/a_2, is about 10:1. Thus, combining both changes in a global 'FRET efficiency' and using this as an indicator of distance variation would lead to incorrect results. Although many FLIM–FRET applications have been described (see [26,28,32] for an overview), there is relatively little information on the application of FLIM–FRET to skin and the molecular interaction of endogenous compounds with the biomolecules in skin.

8. Fluorescence lifetime imaging microscopy applied to skin strata

A major limitation in assessing epithelial condition and topically applied product effectiveness for viable epidermal conditions

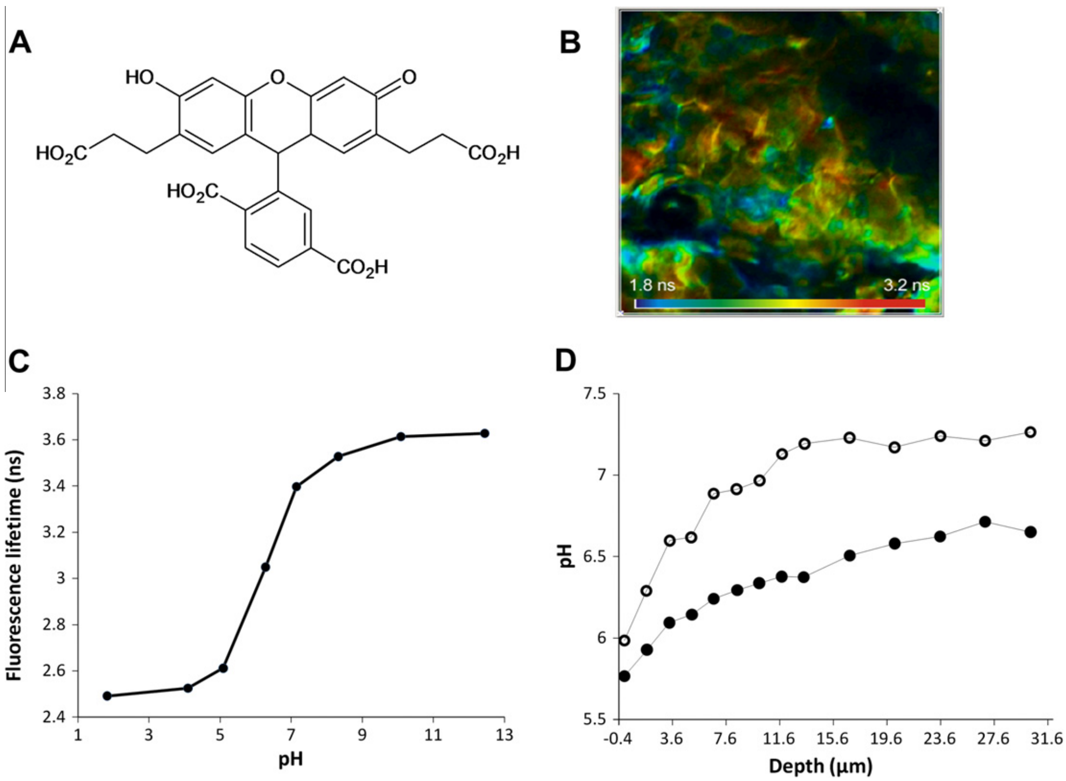

Fig. 7. (A) Chemical formula of the indicator BCECF. (B) Lifetime image of skin tissue stained with BCECF (data courtesy of Theodora Mauro, University of San Francisco, Zeiss LSM 510 NLO with bh SPC-830). The lifetime is an indicator of the pH. (C and D) The fluorescence lifetime of BCECF varies with pH and defines a lower pH at the artificial stratum corneum surface in intercellular lipids (adapted from Niesner et al. [92]).

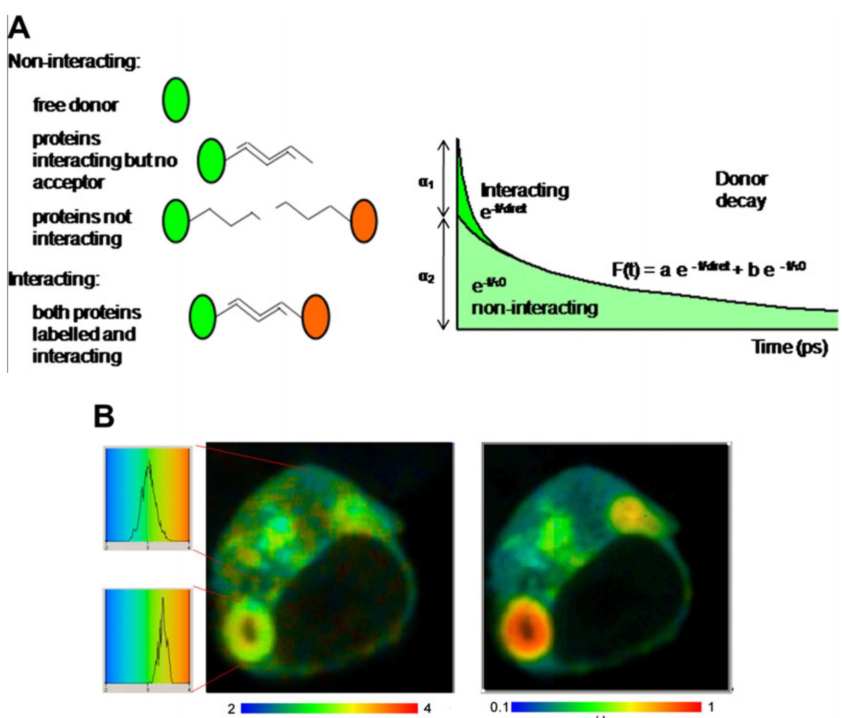

Fig. 8. (A) Fluorescence decay components in FRET systems. (B) FRET results from a cultured human embryonic kidney (HEK) cell obtained by double-exponential lifetime analysis. Left: τ_0/τ_{fret}, Right: N_{fret}/N_0. (Courtesy of Christoph Biskup, University Jena, Institute of Physiology, Germany.) Raw data same as in [29], re-processed. A large number of FLIM–FRET applications have been published in the last few years. For an overview about the FLIM–FRET applications and the related literature, please see [26,28,32].

has been the availability of appropriate methods that can measure *in vivo* epithelial morphology, biochemistry and pathology directly. The combination of confocal or MPM with FLIM offers the opportunity of better understanding the skin [48]. These technologies enable non-invasive optical sectioning of human skin and disease states *in vivo* [23].

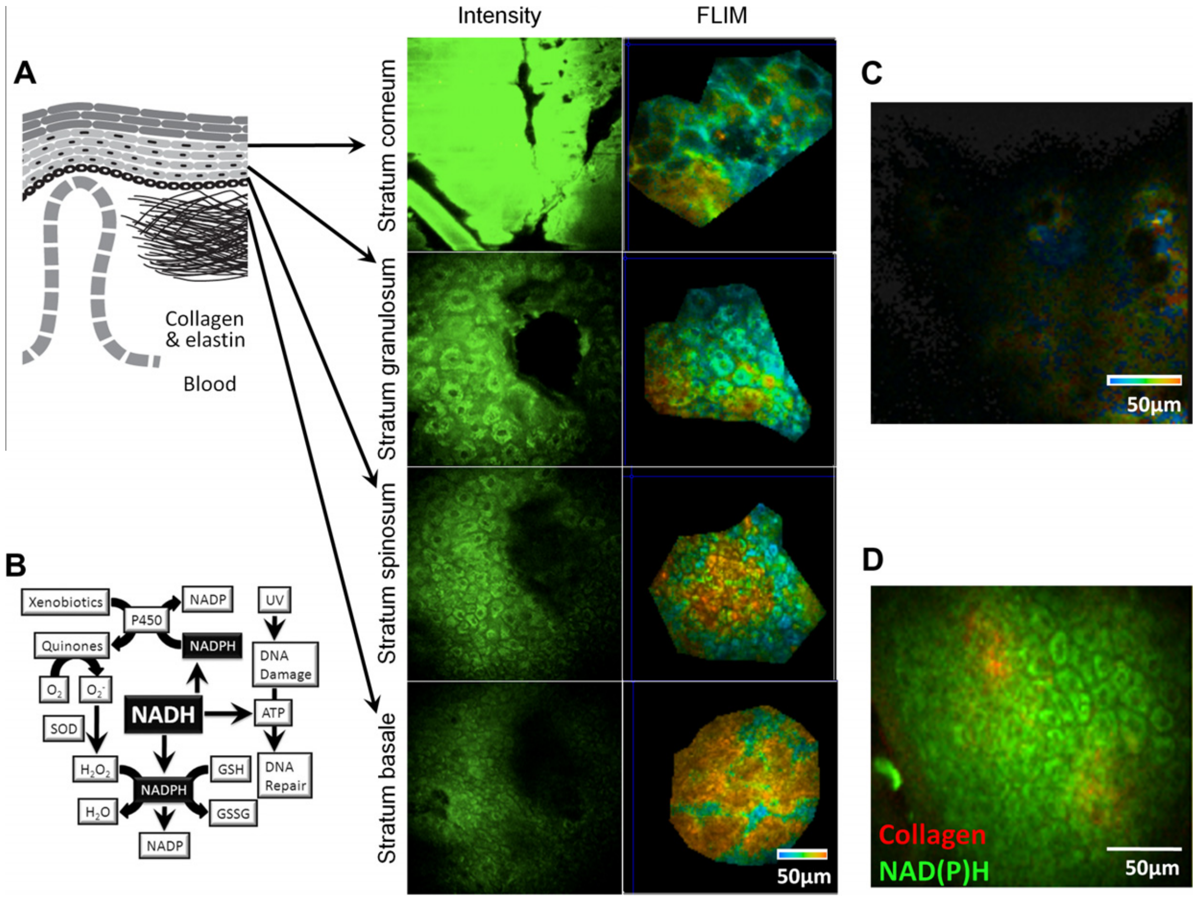

Fig. 9. (A) Schematic illustrating the layers of the skin with dermal collagen and blood flow below as a side view and intensity and FLIM images of the different skin layers *en face*. (B) NAD(P)H is necessary to protect the cell from toxic insults and UV-induced DNA damage. (C) FLIM image showing that very little NAD(P)H signal can be collected from necrotic skin. (D) FLIM image showing the presence of collagen and NAD(P)H at the dermal–epidermal junction with overlaid intensity images taken with 850-nm (red) and 740-nm (green) excitation light.

NAD(P)H is the dominant fluorophore in the viable epidermis and includes both NADH and NADPH, which have indistinguishable fluorescence excitation and emission profiles. Fig. 9A shows FLIM profiles for various epidermal layers. It is evident that there is an increase in longer lifetimes with increasing depth in the epidermis, presumably reflecting an increase in bound NAD(P)H. In contrast, the intensity profiles decrease with distance, possibly reflecting the loss of light due to scattering at the larger depths. As summarized in Fig. 9B, NAD(P)H is critical in maintaining the redox state of the skin and protecting against external insults from xenobiotics and UV light [49,50]. Free NADH can be depleted by (a) binding to metabolic proteins such as lactate dehydrogenase and malate dehydrogenase; (b) use in the electron transport chain to form ATP and in turn enable DNA repair from oxidative stress; and (c) conversion into NAD(P)H, which, in turn, can regulate metabolism, e.g. P450 [46]. As NAD(P)H is one of the major energy sources for intracellular antioxidants that scavenge free radicals, its depletion may lead to impaired metabolism and an increased frequency of DNA mutation [49]. Fig. 9C shows an example of all autofluorescence being lost as a consequence of excised skin being stored or frozen for prolonged periods [51]. The loss of NAD(P)H is faster at higher temperatures and when the skin is frozen [51].

Sugata et al. have recently reported the FLIM of melanin in a human 3D skin model containing melanocytes [52]. We have used FLIM to study melanin in cultured melanocytes, in the hair bulb and in dorsal and volar forearms of a study subject. Melanin was excited with 760- and 800-nm light (1–10 mW), and the emission was collected with a 450 ± 40 nm band-pass filter. The FLIM characteristics of melanin that were reported varied: τ_1 = 97–151 ps, τ_2 = 476–1762 ps and a_1/a_2 = 15–42.

Ionic gradients, calcium in particular, are essential for the maintenance of the epidermal barrier [53]. Investigations into calcium gradients traditionally use fluorescent Ca^{2+}-sensitive dyes, but there are significant problems with this approach: (1) dye concentration artefacts; (2) limited spatial resolution; and (3) thin sections are needed [54,55]. Celli et al. [53] have used MPM-FLIM to overcome many of these issues. However, FLIM analysis and interpretation have additional problems. FLIM data have usually been represented as a histogram (see Fig. 8B, 5). The phasor approach shows a global view of the data where each pixel of the image is represented, using the raw data rather than fitting the fluorescence decay using exponentials [3]. This has a twofold effect; these data are interpreted by the user and analysis is instantaneous because it is a straightforward calculation, not a fitting procedure. In the study by Celli et al., the range in which CG5N was capable of detecting calcium was characterised with FLIM and found to be from 0.5 μM to 20 μM Ca^{2+}.

A special case of FLIM arises when a proteinaceous structure essentially converts, on reflection, two photons of excitation light into a single emission photon. The effect is that the resulting emission wavelength is half of the initial excitation wavelength. This ultrafast process, called second harmonic generation (SHG), generally requires femtosecond pulsed light. In skin, collagen undergoes SHG with 800-nm excitation light and emits 400-nm light and can be used to measure collagen degradation in skin ageing, as discussed later. SHG can be differentiated from the relatively slower process of fluorescence via lifetime measurements where the SHG has an a_1 of 95–100%, in contrast with NAD(P)H fluorescence at a_1 of 40–80%. Fig. 9D shows SHG due to collagen in the protruding dermal papillae as red patches.

Krishnan and Nordlund investigated the fluorescence lifetime properties of three organic sunscreens (octyl salicylate, padimate O and octyl methoxy cinnamate) applied to the skin [56]. Octyl salicylate had a single lifetime component, τ_1, which ranged from 0.14 to 0.46 ns depending on the solvent used. Padimate O had two lifetime components, with $\tau_1 = 1.44$ and 1.61 ns and $\tau_2 = 3.68$ and 3.36 ns in ethyl acetate and toluene, respectively.

A common way to record data in confocal and multiphoton microscopy is to take z-stacks of several images at increasing depth. FLIM is no different. The benefit of FLIM is that fluorescent species, like NAD(P)H and melanin, can be observed and analysed for lifetime and intensity changes on a pixel-by-pixel basis. Fig. 10 shows an example of healthy skin imaged from the stratum corneum (0 μm) to the superficial dermis (90 μm). The top panels show a_1/a_2 ratio pseudo-colouring from 0 to 10, blue to red, which is indicative of metabolic rate, and the red areas suggest melanin or collagen.

Fig. 11 shows images of an excised pig skin sample recorded in two wavelength channels, <480 nm and >480 nm. The <480-nm channel contains both SHG from collagen and NADH fluorescence. The SHG component was extracted from the decay profiles, and the ratio of SHG to fluorescence intensity assigned to the colour. The >480-nm channel shows an image of the amplitude-weighted mean fluorescence lifetime, τ_m.

9. FLIM to study percutaneous penetration

A major challenge in assessing the efficacy of topical products is to derive real-world local efficacy and toxicity data [40,57]. A number of papers have used confocal and multiphoton native fluorescence to describe the penetration of chemicals and nanoparticles [58–62]. In our experience, a combination of multispectral imaging and FLIM is preferred in studying the skin

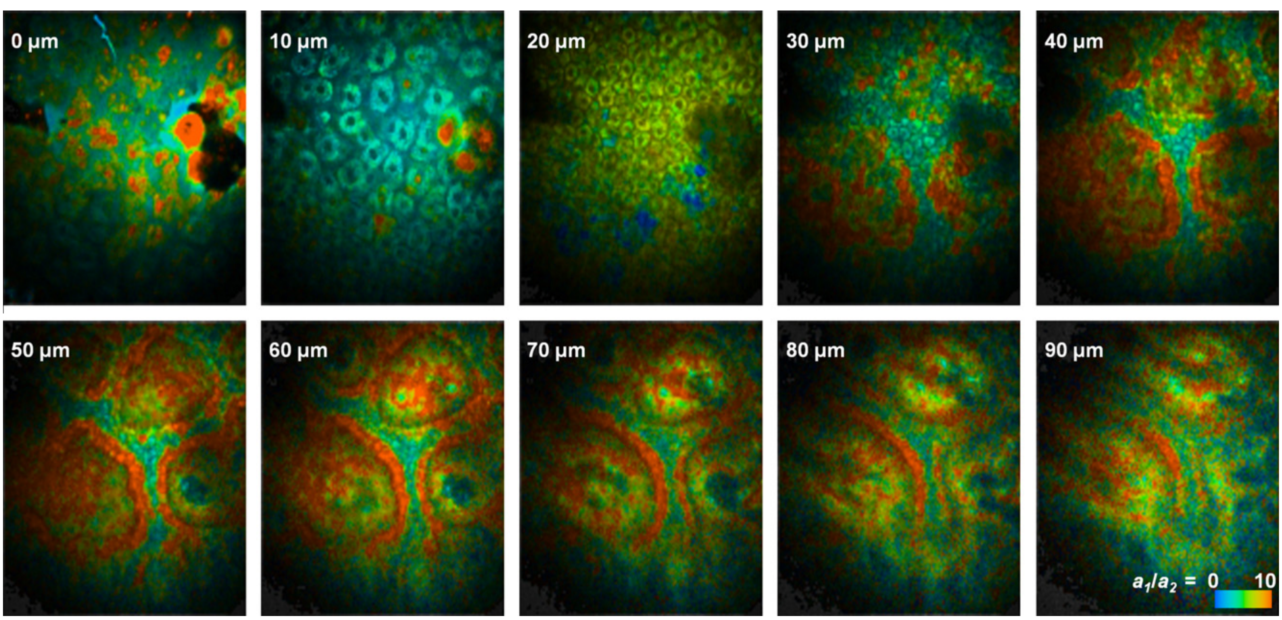

Fig. 10. Healthy human skin imaged from the surface of the stratum corneum (0 μm) to the superficial dermis (90 μm). The papillary rings can be seen starting at 30 μm in red, suggesting the presence of melanin or collagen. Amplitude-weighted mean lifetime of double-exponential decay, a_1/a_2 ratio from 0 to 10, blue to red. The bar indicates the colour scale and 50 μm.

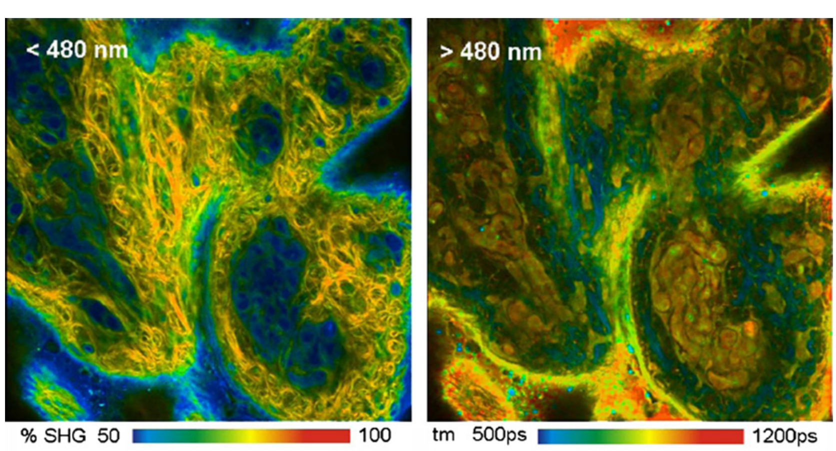

Fig. 11. Two-photon FLIM of pig skin with emission wavelength channel < 480 nm on left with pseudo-colour showing percentage of SHG in the recorded signal and, on right, emission wavelength channel > 480 nm, with pseudo-colour used to show variations in amplitude-weighted mean lifetime, τ_m [28].

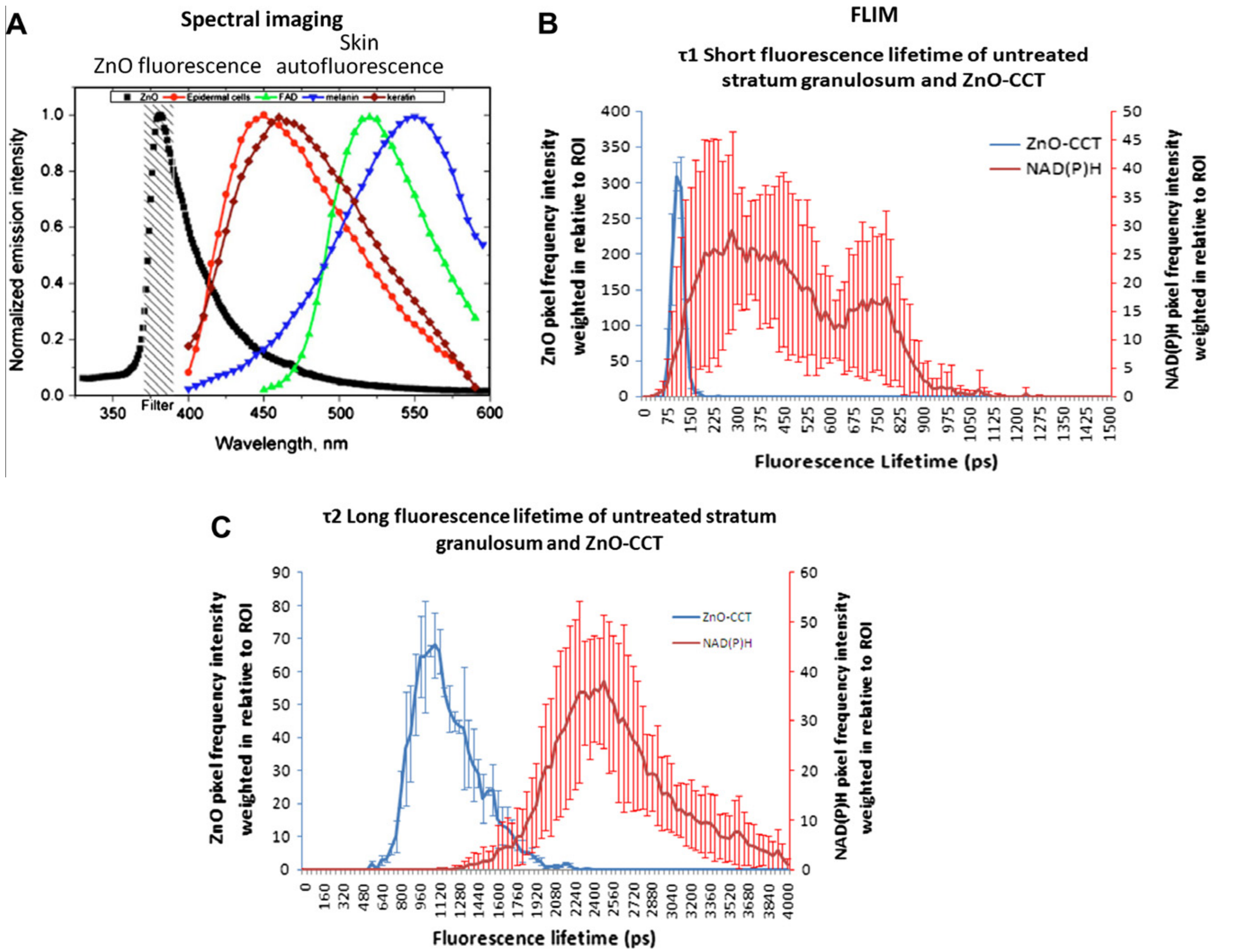

Fig. 12. A comparison of multispectral and FLIM imaging for nanozinc oxide and human epidermis using an excitation wavelength of 740 nm on a titanium–sapphire laser (MaiTai, Spectra Physics) with a laser pulse width of 85 femto-seconds and a repetition rate of 80 megahertz. It is evident that the near band-edge ~380-nm UV photoluminescence of zinc oxide does not overlap with the autofluorescent signals from the various endogenous components in the viable epidermis. On the other hand, it is evident that the other radiative trap-state green (~520 nm) photoluminescence emission will overlap. The short fluorescence life time for the zinc oxide also overlaps with those for endogenous compounds, whereas that the long lifetime of zinc oxide measurable with a Ti:Sa laser shows only a partial overlap with the observed endogenous fluorescence lifetimes.

penetration of xenobiotics and nanoparticles. For instance, Fig. 12 shows our findings for the emission spectra and FLIM for zinc oxide (ZnO) compared with the endogenous autofluorescent skin components. It is evident that there is good separation of the emission spectra for ZnO nanoparticles from the skin autofluorescence but that the FLIM profile for ZnO nanoparticles cannot easily be separated from the dominant NAD(P)H autofluorescence unless the appropriate spectral emission bands are used. Our data in Fig. 12 are consistent with strong UV (~380 nm) photoluminescence near band-edge emission from ZnO, a wide bandgap (3.37 eV) semiconductor with a large exciton binding energy (60 meV) that also shows a size-dependent deep-level or trap-state green light (~520 nm) photoluminescence emission, due to a radiative recombination of a photogenerated hole with an electron occupying the singly ionized oxygen vacancy in ZnO [63]. We showed that uncoated zinc oxide nanoparticles had fluorescence lifetimes of 21 ns, 478 ns and 2.5 μs, whereas ZnO nanocoated with polymethylsilsesquioxane had only the shorter two lifetimes [40]. The ability to use FLIM with zinc oxide is complicated by zinc oxide having a longer fluorescence lifetime than the 75-fs pulse repetition provided by the Ti:Sa fs lasers and its shorter lifetimes of 1.04 ns being similar to keratin and its lifetime of 4.3 ns being comparable with the flavine lifetime of 5.2 ns [40]. Fig. 12 B shows that there is considerable overlap between the short lifetime for zinc oxide and the dominant NAD(P)H autofluorescent lifetime in viable epidermis. More separation is possible with the longer lifetime measurable with a pulse laser but either a limited lifetime band or combined spectral imaging must be used for resolution. We have used the multispectral differences to show that ZnO nanoparticles are retained at the surface and in the upper layers of the stratum corneum on application to human *in vitro* and *in vivo* skin [40,57].

As a second illustration, we have used multispectral imaging and FLIM to study the vesicle delivery of siRNA to the viable epidermis after topical application to excised skin. We found no penetration into excised skin for rigid liposomes but increasing penetration corresponding to the deformability of the liposomes (Fig. 13). It is evident that most penetration occurs via the dermatoglyphs (furrows) with initial evidence that there is transfer of some of the most flexible liposome into deeper tissues and into the cells. Consistent with this apparent transport, there is a change in NAD(P)H lifetimes as shown in the inset of Fig. 13.

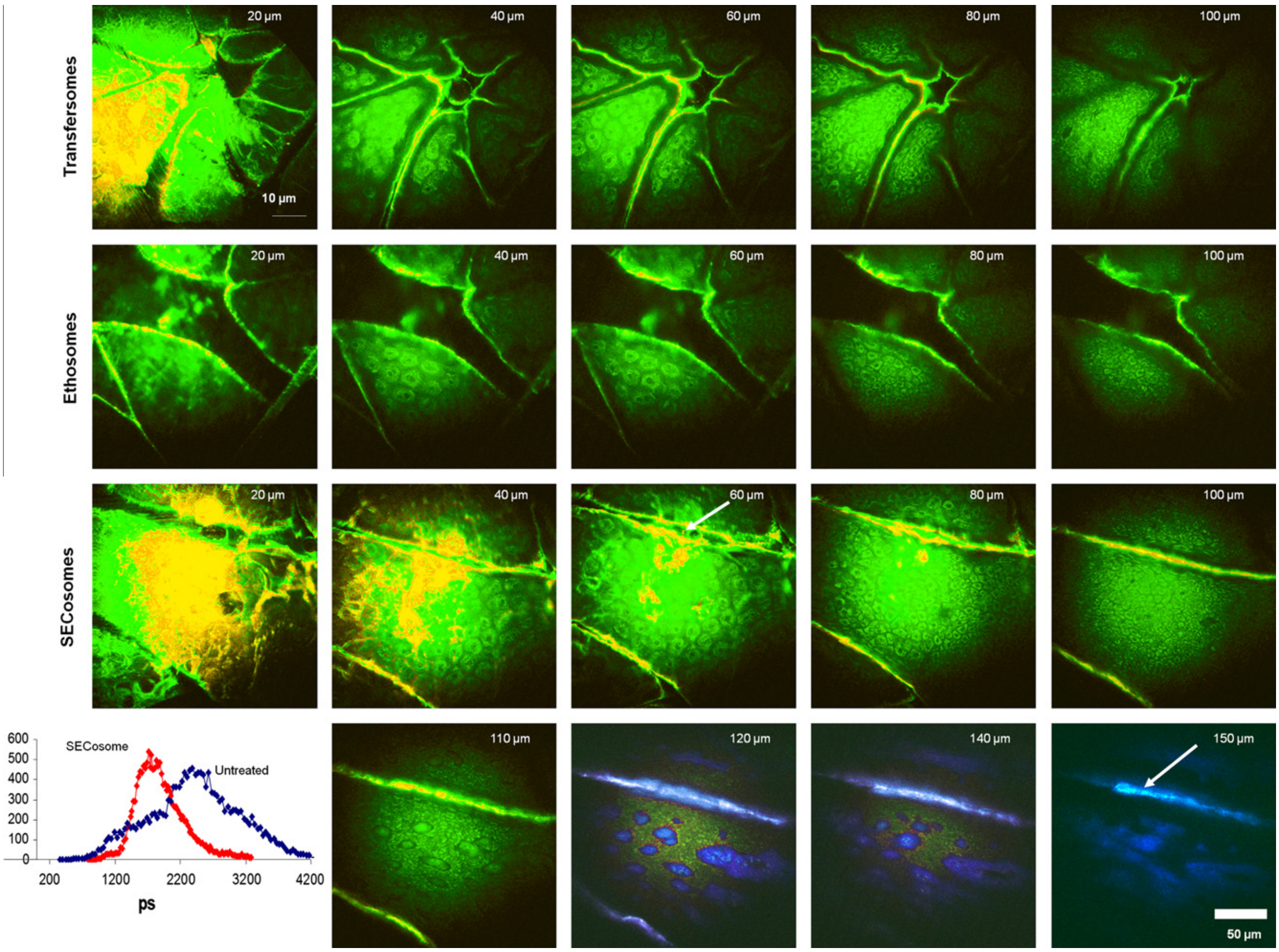

Fig. 13. Penetration of siRNA labelled with 5-carboxyfluorescein (ex494/em520 nm) in flexible liposomes into fresh excised human skin. The sizes of the liposomes and % decrease in size caused by filtration through a 30-nm porous filter were: rigid liposomes 98 ± 2 nm, –; transfersomes 98 ± 2 nm, 30%; ethosomes 79 ± 3 nm, 11%; and secosomes 58 ± 1 nm, 3%. Also shown is the lifetime change in the slow lifetime as a consequence of secosome penetration into the epidermal cells (adapted from Geusens et al. [93]).

10. Skin conditions

The use of FLIM to diagnose various skin conditions is presently at an early stage. We have been examining different skin diseases and present some examples in Fig. 14. It is likely that, as well as combined spectral imaging and FLIM, other complementary modalities such as reflectance and Raman imaging with confocal and multiphoton spectroscopy may be needed to achieve robust diagnostic discrimination between different skin diseases and lesional boundaries. Lin et al. [64] used multiphoton imaging to assess skin ageing in excised, formalin-fixed facial skin and showed that the collagen SHG signal decreased, whereas epidermal autofluorescence increased with skin age. This work was then validated *in vivo* [23]. The ratio of the collagen SHG signal to the epidermal autofluorescence was used to define a parameter SAAID, SHG-to-AF-aging-index-of-dermis, that quantifies the extent of ageing in the skin specimen. Whilst, in principle, this ratio can be used to measure skin ageing with time or loss of collagen in various diseases, its application to quantifying skin ageing appears to be limited at present.

A number of contradictory findings have been reported in attempts to use FLIM for skin disease diagnosis. As an example, Galletly et al. [65] have suggested that FLIM can be used to distinguish basal cell carcinomas (BCC) from uninvolved skin. On the other hand, De Giorgi et al. [48] showed that whilst FLIM is effective in discriminating healthy skin from malignant melanoma, multispectral imaging is more effective in discriminating healthy skin from basal cell carcinomas. They further showed that the detection of the borders for BCCs could be improved using methyl-aminolevulinate as a contrast agent [66]. More recently, the Kaatz group has explored the usefulness of FLIM for melanoma diagnosis [31] and found that aspects of skin morphology, including architectural epidermal disarray, poorly defined keratinocyte cell borders and pleomorphic or dendritic cells presence, were more predictive than FLIM [67]. They also suggested that a fluorescence emission peak at about 560 nm may enable the discrimination of melanomas from naevae [31].

11. Limitations

11.1. General problems of fluorescence measurement in biological samples

Although fluorescence lifetime techniques are inherently independent of the concentration of emitters and absorbers, they cannot solve the problem that the fluorescence behaviour of biological samples does not depend only on a single parameter. There may be competing quenching mechanisms, inhomogeneity in fluorophore binding, variations in viscosity and refractive index or just unwanted contributions from other fluorophores. The quantitative analysis of FLIM data thus requires a reasonably

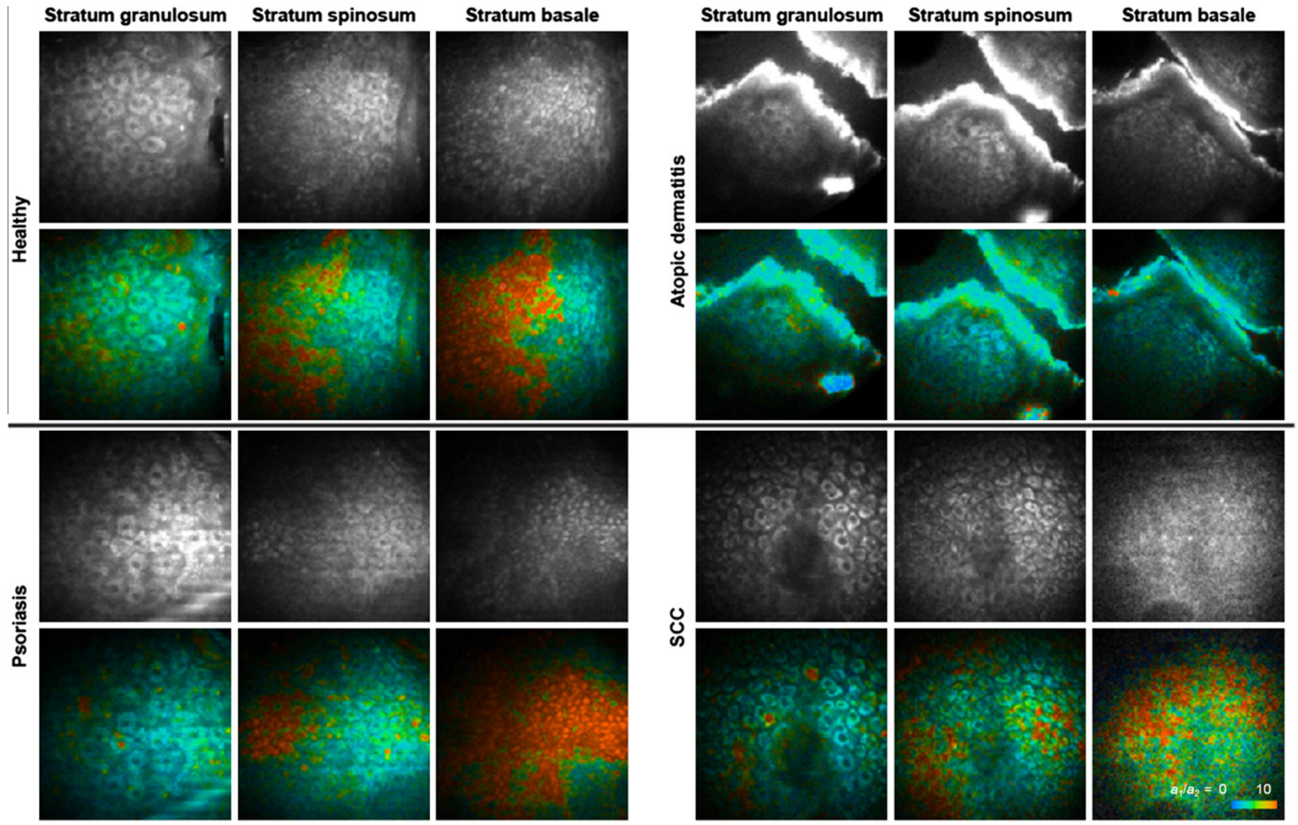

Fig. 14. Examples of FLIM z-stacks from healthy, psoriasis lesional, atopic dermatitis lesional and squamous cell carcinoma (SCC) lesional skin. Both the intensity image (top, gray scale) and FLIM (bottom, colour) images are shown for the stratum granulosum, stratum spinosum and stratum basale. The NAD(P)H FLIM images are pseudo-coloured from a_1/a_2 = 0 to 10, in blue to red, as an indication of metabolic rate. Both the morphology (intensity images) and the metabolic rates differ depending on the condition. The NAD(P)H a_1/a_2 ratio is inversely related to the metabolic rate. The bar indicates the colour scale and 50 µm.

accurate model of the conditions in the sample, the number of decay components to be expected and the parameters influencing their lifetimes.

Even if a suitable model is available, it is important that photobleaching of the fluorophores be kept at a negligible level. At first glance, photobleaching may be considered without influence on the fluorescence lifetimes of the remaining fluorophore molecules. Unfortunately in practice, this is not the case. Different fluorophores and/or different fractions of the same fluorophore photobleach at different rates. Fluorophores may also undergo photoconversion, i.e. develop changes in the fluorescence spectra and fluorescence lifetimes on illumination. Finally, photobleaching may create radicals that are toxic to the cells and induce changes in the structure of proteins or in metabolism. Sample exposure must therefore be kept as low as possible. However, these issues are not restricted to fluorescence lifetime techniques. They are inherent to any molecular imaging technique in biology. Steady-state techniques have to deal with the same problems.

11.2. Acquisition time

A problem in clinical application is the relatively long acquisition times needed to obtain good FLIM results. Reasonable FLIM data are obtained within a few seconds; high-accuracy FLIM can require more than one minute. If FLIM z-stacks are to be recorded, the total acquisition time becomes unacceptably long.

It should be noted here that long acquisition times are *not* a feature of FLIM in general or TCSPC FLIM in particular. There is a given relation between the standard deviation of the lifetimes and the number of photons recorded [68]. Consequently, shorter acquisition times can only be achieved by increasing the detected photon rate. The photon rate for *in vivo* applications is, however, limited by photobleaching and photodamage effects. The available photon rate is currently well within the counting capability of the TCSPC module. Thus, technical efforts to increase the throughput of the FLIM electronics, i.e. by parallel operation of several modules [26,69], would not immediately result in a reduction in the acquisition time. An improvement can, however, be expected from new detector principles that combine high efficiency with large-area detection [70].

11.3. NADH/FAD fluorescence

One of the challenges of metabolic FLIM is the separation of NADH and FAD fluorescence. There is neither an excitation nor an emission wavelength at which NADH fluorescence can be detected without contamination by FAD fluorescence. This makes it difficult to interpret changes in the decay profiles recorded. Improvements can be obtained by multispectral FLIM and spectral and temporal unmixing of the components. This is difficult because additional fluorophores and absorbers of unknown absorption and emission spectra may be present. Software approaches to solve these problems are described in [17,71]. On the hardware side, multiplexing of several excitation wavelengths and multiplexed TCSPC operation [26,28] may help obtain better discrimination of the fluorophores.

11.4. Interpretation of the data

Even with NADH fluorescence signals reasonably separated from other emissions, the interpretation is still controversial. At the moment, the approaches are semi-empirical: Measurements are taken on as many patients and tissue lesions as possible and spectroscopic signatures are sought.

11.5. Ease of instrument use

The current instrument is cumbersome to use on humans. Improvements are expected from integration of a flexible arm that increases flexibility by placing the detection system on the patient. Other improvements could be obtained by better communication of the scan control and the FLIM acquisition software as in the case of the instrument described in [32].

11.6. Speed of data analysis

Depending on the number of pixels and time channels, currently used fitting procedures need between 10 s to several minutes to analyse a single FLIM image. Analysis of large numbers of images is thus time-consuming. Improvements could be obtained by batch processing or by analysis of the TCSPC FLIM data in the frequency domain [72].

11.7. Non-fluorescent molecules

A major limitation of using FLIM to address the challenge of how to study the skin penetration of compounds non-invasively in man *in vivo* is the requirement that the molecules must be fluorescent. In reality, autofluorescence and optical limitations effectively further limit the range of solutes that can be studied to those fluorescent solutes that are excited at wavelengths of generally greater than 350 nm. This limitation excludes a large number of fluorescent molecules, especially those which are small in size and of interest from a percutaneous penetration perspective. Confocal microscopy – Raman spectroscopy – has been advocated as one way forward but, in our experience, it has a major limitation in sensitivity for many molecules in skin *in vivo*. Thus, the challenge remains. How can we study the penetration of the wide range of compounds applied topically in man *in vivo* and examine epidermal concentrations non-invasively?

12. Summary

Fluorescence lifetime imaging (FLIM) is a direct way of obtaining information about molecular interactions in biological cells and tissue. In combination with multiphoton excitation, non-descanned detection and simultaneous recording of signals in several wavelength channels, FLIM delivers images of fluorescence decay parameters of multiple fluorophores from depths of up to 200 μm in tissue. The data recorded can be used to sense local environment parameters, such as pH, ion concentrations or local viscosity.

A substantial advantage of FLIM over steady-state imaging techniques results from the ability to discriminate fractions of the same fluorophore in different states of interaction with its molecular environment. In Förster Resonance Energy Transfer (FRET) experiments, FLIM not only detects FRET without the need of correcting spectral bleedthrough effects, but is also able to discriminate bound and unbound donor fractions. It is thus possible to separate the effects of variable distance and the ratio of interacting to non-interacting protein fractions in protein interaction experiments.

The ability to detect and to separate signals from different states of the same fluorophore has also led to a breakthrough in autofluorescence imaging. Most of the endogenous fluorophores exist in bound and unbound states or in slightly different conformations. FLIM is able to resolve these fractions and thus obtain biological information not accessible by steady-state imaging techniques. Presently, autofluorescence FLIM techniques and the corresponding instruments are at the threshold of clinical application and mainly used in research. Results are not always easy to interpret and often controversial. Advances into clinical diagnostics require more data, better insight into physiological processes at the molecular level and closer interaction between clinical research teams and instrument designers.

Acknowledgements

We thank the Queensland Cancer Fund, the National Health & Medical Research Council of Australia and United States Air Force, Asian Office of Aerospace Research & Development for their support.

References

[1] M. Göppert-Mayer, Über Elementarakte mit zwei Quantensprüngen, Ann. Phys. 4031 (1931) 273–294.
[2] W. Denk, J.H. Strickler, W.W. Webb, 2-Photon laser scanning fluorescence microscopy, Science 248 (1990) 73–76.
[3] A. Diaspro, Confocal and Two-photon Microscopy: Foundations, Applications and Advances, Wiley-Liss, 2001.
[4] J. Pawley, Handbook of Biological Confocal Microscopy, Springer, 2006.
[5] J.R. Lakowicz, Principles of Fluorescence Spectroscopy, Springer, New York, 2006.
[6] Y. Yamaguchi, Y. Matsubara, T. Ochi, T. Wakamiya, Z.I. Yoshida, How the pi conjugation length affects the fluorescence emission efficiency, J. Am. Chem. Soc. 130 (2008) 13867–13869.
[7] K. Funk, A. Woitecki, C. Franjic-Wurtz, T. Gensch, F. Mohrlen, S. Frings, Modulation of chloride homeostasis by inflammatory mediators in dorsal root ganglion neurons, Mol. Pain. 4 (2008).
[8] D. Gilbert, C. Franjic-Wurtz, K. Funk, T. Gensch, S. Frings, F. Mohrlen, Differential maturation of chloride homeostasis in primary afferent neurons of the somatosensory system, Int. J. Dev. Neurosci. 25 (2007) 479–489.
[9] H. Kaneko, I. Putzier, S. Frings, U.B. Kaupp, T. Gensch, Chloride accumulation in mammalian olfactory sensory neurons, J. Neurosci. 24 (2004) 7931–7938.
[10] K.V. Kuchibhotla, C.R. Lattarulo, B.T. Hyman, B.J. Bacskai, Synchronous hyperactivity and intercellular calcium waves in astrocytes in Alzheimer mice, Science 323 (2009) 1211–1215.
[11] B. Chance, Pyridine–nucleotide as an indicator of oxygen requirements for energy-linked functions of mitochondria, Circ. Res. 38 (1976) 31–38.
[12] B. Chance, B. Schoener, R. Oshino, F. Itshak, Y. Nakase, Oxidation–reduction ratio studies of mitochondria in freeze-trapped samples – NADH and flavoprotein fluorescence signals, J. Biol. Chem. 254 (1979) 4764–4771.
[13] D. Schweitzer, S. Schenke, M. Hammer, F. Schweitzer, S. Jentsch, E. Birckner, W. Becker, A. Bergmann, Towards metabolic mapping of the human retina, Microsc. Re.s Tech. 70 (2007) 410–419.
[14] J.R. Lakowicz, H. Szmacinski, K. Nowaczyk, M.L. Johnson, Fluorescence lifetime imaging of free and protein-bound NADH, Proc. Natl. Acad. Sci. USA 89 (1992) 1271–1275.
[15] R.J. Paul, H. Schneckenburger, Oxygen concentration and the oxidation–reduction state of yeast: determination of free/bound NADH and flavins by time-resolved spectroscopy, Naturwissenschaften 83 (1996) 32–35.
[16] D.K. Bird, L. Yan, K.M. Vrotsos, K.W. Eliceiri, E.M. Vaughan, P.J. Keely, J.G. White, N. Ramanujam, Metabolic mapping of MCF10A human breast cells via multiphoton fluorescence lifetime imaging of the coenzyme NADH, Cancer Res. 65 (2005) 8766–8773.
[17] D. Chorvat, A. Chorvatova, Multi-wavelength fluorescence lifetime spectroscopy: a new approach to the study of endogenous fluorescence in living cells and tissues, Laser Phys. Lett. 6 (2009) 175–193.
[18] V.V. Ghukasyan, F.J. Kao, Monitoring cellular metabolism with fluorescence lifetime of reduced nicotinamide adenine dinucleotide, J. Phys. Chem. C 113 (2009) 11532–11540.
[19] M.C. Skala, K.M. Riching, D.K. Bird, A. Gendron-Fitzpatrick, J. Eickhoff, K.W. Eliceiri, P.J. Keely, N. Ramanujam, In vivo multiphoton fluorescence lifetime imaging of protein-bound and free nicotinamide adenine dinucleotide in normal and precancerous epithelia, J. Biomed. Opt. 12 (2007).
[20] K.M. Hanson, M.J. Behne, N.P. Barry, T.M. Mauro, E. Gratton, R.M. Clegg, Two-photon fluorescence lifetime imaging of the skin stratum corneum pH gradient, Biophys. J. 83 (2002) 1682–1690.
[21] T. Förster, Zwischenmolekulare Energiewanderung und Fluoreszenz, Ann. Phys. 457 (1948) 55–75.
[22] B.R. Masters, P.T.C. So, Handbook of Biomedical Nonlinear Optical Microscopy, Oxford University Press, 2008.
[23] M.J. Koehler, K. Konig, P. Elsner, R. Buckle, M. Kaatz, In vivo assessment of human skin aging by multiphoton laser scanning tomography, Opt. Lett. 31 (2006) 2879–2881.
[24] I. Bugiel, K. König, H. Wabnitz, Investigation of cells by fluorescence laser scanning microscopy with subnanosecond time resolution, Lasers Life Sci. 3 (1989) 1–7.
[25] K. Konig, Clinical multiphoton tomography, J. Biophoton. 1 (2008) 13–23.
[26] W. Becker, The bh TCSPC handbook, fourth ed., Becker & Hickl GmbH, Berlin, 2010. <http://www.becker-hickl.com>.

[27] W. Becker, A. Bergmann, Lifetime-resolved imaging in nonlinear microscopy, in: B.R. Masters, P.T.C. So (Eds.), Handbook of Biomedical Nonlinear Optical Microscopy, Oxford University Press, 2008.
[28] W. Becker, Advanced Time-correlated Single-photon Counting Techniques, Springer, Berlin, Heidelberg, New York, 2005.
[29] W. Becker, A. Bergmann, M.A. Hink, K. Konig, K. Benndorf, C. Biskup, Fluorescence lifetime imaging by time-correlated single-photon counting, Microsc. Res. Tech. 63 (2004) 58–66.
[30] W. Becker, A. Bergmann, C. Biskup, Multispectral fluorescence lifetime imaging by TCSPC, Microsc. Res. Tech. 70 (2007) 403–409.
[31] E. Dimitrow, I. Riemann, A. Ehlers, M.J. Koehler, J. Norgauer, P. Elsner, K. Konig, M. Kaatz, Spectral fluorescence lifetime detection and selective melanin imaging by multiphoton laser tomography for melanoma diagnosis, Exp. Dermatol. 18 (2009) 509–515.
[32] Becker & Hickl GmbH, DCS-120 Confocal Scanning FLIM Systems, User Handbook, 2009.s<http://www.becker-hickl.com>.
[33] D. Schweitzer, Quantifying fundus autofluorescence, in: N. Lois, J.V. Forrester (Eds.), Fundus Autofluorescence, Wolters Kluwer, Lippincott Williams & Wilkins, 2009.
[34] T. Wilson, C. Sheppard, Theory and Practice of Scanning Optical Microscopy, Academic Press, 1984.
[35] K. Konig, Multiphoton microscopy in life sciences, J. Microsc. (Oxford) 200 (2000) 83–104.
[36] T.H. Chia, A. Williamson, D.D. Spencer, M.J. Levene, Multiphoton fluorescence lifetime imaging of intrinsic fluorescence in human and rat brain tissue reveals spatially distinct NADH binding, Opt. Exp. 16 (2008) 4237–4249.
[37] R.F. de Almeida, J. Borst, A. Fedorov, M. Prieto, A.J. Visser, Complexity of lipid domains and rafts in giant unilamellar vesicles revealed by combining imaging and microscopic and macroscopic time-resolved fluorescence, Biophys. J. 93 (2007) 539–553.
[38] M.Y. Berezin, S. Achilefu, Fluorescence lifetime measurements and biological imaging, Chem. Rev. 110 (2010) 2641–2684.
[39] D. Grotte, V. Mattox, R. Brubaker, Fluorescent, physiological and pharmacokinetic properties of fluorescein glucuronide, Exp. Eye Res. 40 (1985) 23–33.
[40] M.S. Roberts, M.J. Roberts, T.A. Robertson, W. Sanchez, C. Thorling, Y.H. Zou, X. Zhao, W. Becker, A.V. Zvyagin, In vitro and in vivo imaging of xenobiotic transport in human skin and in the rat liver, J. Biophoton. 1 (2008) 478–493.
[41] K.M. Hanson, N.P. Barry, M.J. Behne, T.M. Mauro, E. Gratton, R.M. Clegg, Two-photon fluorescence lifetime imaging of the skin's stratum corneum pH gradient, Biophys. J. 82 (2002) 494a.
[42] A. Periasamy, Methods in Cellular Imaging, first ed., Oxford University Press, Oxford, New York, 2001.
[43] C. Biskup, L. Kelbauskas, T. Zimmer, K. Benndorf, A. Bergmann, W. Becker, J.P. Ruppersberg, C. Stockklausner, N. Klocker, Interaction of PSD-95 with potassium channels visualized by fluorescence lifetime-based resonance energy transfer imaging, J. Biomed. Opt. 9 (2004) 753–759.
[44] Y.E. Chen, A. Periasamy, Characterization of two-photon excitation fluorescence lifetime imaging microscopy for protein localization, Microsc. Res. Tech. 63 (2004) 72–80.
[45] S. Pelet, M.J.R. Previte, P.T.C. So, Comparing the quantification of Forster resonance energy transfer measurement accuracies based on intensity, spectral, and lifetime imaging, J. Biomed. Opt. 11 (2006).
[46] B.J. Bacskai, J. Skoch, G.A. Hickey, R. Allen, B.T. Hyman, Fluorescence resonance energy transfer determinations using multiphoton fluorescence lifetime imaging microscopy to characterize amyloid-beta plaques, J. Biomed. Opt. 8 (2003) 368–375.
[47] M. Peter, S.M. Ameer-Beg, Imaging molecular interactions by multiphoton FLIM, Biol. Cell 96 (2004) 231–236.
[48] V. De Giorgi, D. Massi, S. Sestini, R. Cicchi, F.S. Pavone, T. Lotti, Combined non-linear laser imaging (two-photon excitation fluorescence microscopy, fluorescence lifetime imaging microscopy, multispectral multiphoton microscopy) in cutaneous tumours: first experiences, J. Eur. Acad. Dermatol. 23 (2009) 314–316.
[49] J. Chaudiere, R. Ferrari-Iliou, Intracellular antioxidants: from chemical to biochemical mechanisms, Food Chem. Toxicol. 37 (1999) 949–962.
[50] D. Voet, J.G. Voet, Biochemistry, third ed., Wiley, 2004.
[51] W.Y. Sanchez, T.W. Prow, W.H. Sanchez, J.E. Grice, M.S. Roberts, Analysis of the metabolic deterioration of ex vivo skin from ischemic necrosis through the imaging of intracellular NAD(P)H by multiphoton tomography and fluorescence lifetime imaging microscopy, J. Biomed. Opt. 15 (2010).
[52] K. Sugata, S. Sakai, N. Noriaki, O. Osanai, T. Kitahara, Y. Takema, Imaging of melanin distribution using multiphoton autofluorescence decay curves, Skin Res. Technol. 16 (2010) 55–59.
[53] A. Celli, S. Sanchez, M. Behne, T. Hazlett, E. Gratton, T. Mauro, The epidermal Ca^{2+} gradient: measurement using the phasor representation of fluorescent lifetime imaging, Biophys. J. 98 (2010) 911–921.
[54] M. Tsutsumi, S. Denda, K. Inoue, K. Ikeyama, M. Denda, Calcium ion gradients and dynamics in cultured skin slices of rat hindpaw in response to stimulation with ATP, J. Invest. Dermatol. 129 (2009) 584–589.
[55] M. Denda, T. Tsuchiya, P.M. Elias, K.R. Feingold, Stress alters cutaneous permeability barrier homeostasis, Am. J. Physiol. Regul. Integr. Comp. Physiol. 278 (2000) R367–R372.
[56] R. Krishnan, T.M. Nordlund, Fluorescence dynamics of three UV-B sunscreens, J. Fluoresc. 18 (2008) 203–217.
[57] A.V. Zvyagin, X. Zhao, A. Gierden, W. Sanchez, J.A. Ross, M.S. Roberts, Imaging of zinc oxide nanoparticle penetration in human skin in vitro and in vivo, J. Biomed. Opt. 13 (2008).
[58] R. Alvarez-Roman, A. Naik, Y.N. Kalia, H. Fessi, R.H. Guy, Visualization of skin penetration using confocal laser scanning microscopy, Eur. J. Pharm. Biopharm. 58 (2004) 301–316.
[59] D.C. Carrer, C. Vermehren, L.A. Bagatolli, Pig skin structure and transdermal delivery of liposomes: a two photon microscopy study, J. Controlled Rel. 132 (2008) 12–20.
[60] B.S. Grewal, A. Naik, W.J. Irwin, G. Gooris, G.J. de Grauw, H.G. Gerritsen, J.A. Bouwstra, Transdermal macromolecular delivery: real-time visualization of iontophoretic and chemically enhanced transport using two-photon excitation microscopy, Pharm. Res. 17 (2000) 788–795.
[61] F. Stracke, B. Weiss, C.M. Lehr, K. Koenig, U.F. Schaefer, M. Schneider, Multiphoton microscopy for the investigation of dermal penetration of nanoparticle-borne drugs, J. Invest. Dermatol. 126 (2006) 2224–2233.
[62] B. Yu, C.Y. Dong, P.T.C. So, D. Blankschtein, R. Langer, In vitro visualization and quantification of oleic acid induced changes in transdermal transport using two-photon fluorescence microscopy, J. Invest. Dermatol. 117 (2001) 16–25.
[63] M. Huang, Y. Wu, H. Feick, N. Tran, E. Weber, P. Yang, Catalytic growth of zinc oxide nanowires by vapor transport, Adv. Mater. 13 (2001) 113–116.
[64] S.J. Lin, R.J. Wu, H.Y. Tan, W. Lo, W.C. Lin, T.H. Young, C.J. Hsu, J.S. Chen, S.H. Jee, C.Y. Dong, Evaluating cutaneous photoaging by use of multiphoton fluorescence and second-harmonic generation microscopy, Opt. Lett. 30 (2005) 2275–2277.
[65] N.P. Galletly, J. McGinty, C. Dunsby, F. Teixeira, J. Requejo-Isidro, I. Munro, D.S. Elson, M.A.A. Neil, A.C. Chu, P.M.W. French, G.W. Stamp, Fluorescence lifetime imaging distinguishes basal cell carcinoma from surrounding uninvolved skin, Brit. J. Dermatol. 159 (2008) 152–161.
[66] R. Cicchi, S. Sestini, V. De Giorgi, D. Massi, T. Lotti, F.S. Pavone, Nonlinear laser imaging of skin lesions, J. Biophoton. 1 (2008) 62–73.
[67] E. Dimitrow, M. Ziemer, M.J. Koehler, J. Norgauer, K. Konig, P. Elsner, M. Kaatz, Sensitivity and specificity of multiphoton laser tomography for in vivo and ex vivo diagnosis of malignant melanoma, J. Invest. Dermatol. 129 (2009) 1752–1758.
[68] M. Kollner, J. Wolfrum, How many photons are necessary for fluorescence-lifetime measurements, Chem. Phys. Lett. 200 (1992) 199–204.
[69] W. Becker, B. Su, A. Bergmann, Fast-acquisition multispectral FLIM by parallel TCSPC, Proc. SPIE 7183 (2009).
[70] W. Becker, B. Su, A. Bergmann, Better FLIM and FCS data by GaAsP hybrid detectors, Proc. SPIE 7569 (2010).
[71] D. Chorvat, A. Chorvatova, Spectrally resolved time-correlated single photon counting: a novel approach for characterization of endogenous fluorescence in isolated cardiac myocytes, Eur. Biophys. J. Biophys. 36 (2006) 73–83.
[72] M.A. Digman, V.R. Caiolfa, M. Zamai, E. Gratton, The phasor approach to fluorescence lifetime imaging analysis, Biophys. J. 94 (2008) L14–L16.
[73] E. Brown, T. McKee, E. diTomaso, A. Pluen, B. Seed, Y. Boucher, R.K. Jain, Dynamic imaging of collagen and its modulation in tumors in vivo using second-harmonic generation, Nat. Med. 9 (2003) 796–800.
[74] L.H. Laiho, S. Pelet, T.M. Hancewicz, P.D. Kaplan, P.T.C. So, Two-photon 3-D mapping of ex vivo human skin endogenous fluorescence species based on fluorescence emission spectra, J. Biomed. Opt. 10 (2005).
[75] A. Zoumi, A. Yeh, B.J. Tromberg, Imaging cells and extracellular matrix in vivo by using second-harmonic generation and two-photon excited fluorescence, Proc. Natl. Acad. Sci. USA 99 (2002) 11014–11019.
[76] K. Dowling, M.J. Dayel, M.J. Lever, P.M.W. French, J.D. Hares, A.K.L. Dymoke-Bradshaw, Fluorescence lifetime imaging with picosecond resolution for biomedical applications, Opt. Lett. 23 (1998) 810–812.
[77] P.A.A. De Beule, C. Dunsby, N.P. Galletly, G.W. Stamp, A.C. Chu, U. Anand, P. Anand, C.D. Benham, A. Naylor, P.M.W. French, A hyperspectral fluorescence lifetime probe for skin cancer diagnosis, Rev. Sci. Instrum. 78 (2007).
[78] R. Eichhorn, G. Wessler, M. Scholz, D. Leupold, G. Stankovic, S. Buder, M. Stucker, K. Hoffmann, Early diagnosis of melanotic melanoma based on laser-induced melanin fluorescence, J. Biomed. Opt. 14 (2009).
[79] N. Nakashima, K. Yoshihara, F. Tanaka, K. Yagi, Picosecond fluorescence lifetime of the coenzyme of D-amino-acid oxidase, J. Biol. Chem. 255 (1980) 5261–5263.
[80] A. Ehlers, I. Riemann, M. Stark, K. Konig, Multiphoton fluorescence lifetime imaging of human hair, Microsc. Res. Tech. 70 (2007) 154–161.
[81] A.M. Pena, M. Strupler, T. Boulesteix, M.C. Schanne-Klein, Spectroscopic analysis of keratin endogenous signal for skin multiphoton microscopy, Opt. Exp. 13 (2005) 6268–6274.
[82] B.R. Masters, P.T.C. So, E. Gratton, Multiphoton excitation fluorescence microscopy and spectroscopy of in vivo human skin, Biophys. J. 72 (1997) 2405–2412.
[83] R. Niesner, B. Peker, P. Schlusche, K.H. Gericke, Noniterative biexponential fluorescence lifetime imaging in the investigation of cellular metabolism by means of NAD(P)H autofluorescence, ChemPhysChem 5 (2004) 1141–1149.
[84] R. Cubeddu, A. Pifferi, P. Taroni, A. Torricelli, G. Valentini, F. Rinaldi, E. Sorbellini, Fluorescence lifetime imaging: an application to the detection of skin tumors, IEEE J. Sel. Top Quant. 5 (1999) 923–929.
[85] H. Schneckenburger, K. Konig, K. Kunzirapp, C. Westphalfrosch, A. Ruck, Time-resolved in-vivo fluorescence of photosensitizing porphyrins, J. Photochem. Photobiol. B 21 (1993) 143–147.

[86] M. Collini, B. Leo, G. Baldini, H.L. Monaco, M. Galliano, Probing protein aggregation by time-resolved fluorescence during beta-lactoglobulin crystal growth, Eur. Biophys. J. Biophys. 31 (2002) 111–117.
[87] W.R. Zipfel, R.M. Williams, R. Christie, A.Y. Nikitin, B.T. Hyman, W.W. Webb, Live tissue intrinsic emission microscopy using multiphoton-excited native fluorescence and second harmonic generation, Proc. Natl. Acad. Sci. USA 100 (2003) 7075–7080.
[88] Q.W. Wang, J.C. Allen, H.E. Swaisgood, Binding of vitamin D and cholesterol to beta-lactoglobulin, J. Dairy Sci. 80 (1997) 1054–1059.
[89] M. Hammer, D. Schweitzer, S. Richter, E. Konigsdorffer, Sodium fluorescein as a retinal pH indicator?, Physiol Meas. 26 (2005) N9–N12.
[90] D. Magde, G.E. Rojas, P.G. Seybold, Solvent dependence of the fluorescence lifetimes of xanthene dyes, Photochem. Photobiol. 70 (1999) 737–744.
[91] M. Larsen, L.B.A. Johansson, Time-resolved fluorescence properties of fluorescein and fluorescein glucuronide, Exp. Eye Res. 48 (1989) 477–485.
[92] R. Niesner, B. Peker, P. Schlusche, K.H. Gericke, C. Hoffmann, D. Hahne, C. Muller-Goymann, 3D-resolved investigation of the pH gradient in artificial skin constructs by means of fluorescence lifetime imaging, Pharm. Res. 22 (2005) 1079–1087.
[93] B. Geusens, M. Van Gele, S. Braat, S.C. De Smedt, M.C.A. Stuart, T. Prow, W. Sanchez, M.S. Roberts, N.N. Sanders, J. Lambert, Flexible nanosomes (SECosomes) enable efficient siRNA delivery in cultured primary skin cells and in viable epidermis of ex-vivo human skin, Adv. Funct. Mater. 20 (2010) 4077–4090.